IOP Publishing | International Atomic Energy Agency Nuclear Fusion

Nucl. Fusion **55** (2015) 083021 (24pp) doi:10.1088/0029-5515/55/8/083021

Nonlinear burn condition control in tokamaks using isotopic fuel tailoring

Mark D. Boyer[1,2] **and Eugenio Schuster**[1]

[1] Department of Mechanical Engineering and Mechanics Lehigh University, Bethlehem, PA 18015, USA

E-mail: mboyer@pppl.gov

Received 16 February 2015, revised 21 May 2015
Accepted for publication 10 June 2015
Published 21 July 2015

Abstract

One of the fundamental problems in tokamak fusion reactors is how to control the plasma density and temperature in order to regulate the amount of fusion power produced by the device. Control of these parameters will be critical to the success of burning plasma experiments like ITER. The most previous burn condition control efforts use either non-model based control designs or techniques based on models linearized around particular operating points. Such strategies limit the potential operational space and must be carefully retuned or redesigned to accommodate changes in operating points or plasma parameters. In this work, a nonlinear dynamic model of the spatial averages of energy and ion species densities is used to synthesize a nonlinear feedback controller for stabilizing the burn condition. The nonlinear model-based control strategy guarantees a much larger operational space than previous linear controllers. Because it is not designed around a particular operating point, the controller can be used to move from one burn condition to another. The proposed scheme first attempts to use regulation of the auxiliary heating power to reject temperature perturbations, then, if necessary, uses isotopic fuel tailoring as a way to reduce fusion heating during positive temperature perturbations. A global model of hydrogen recycling is incorporated into the model used for design and simulation, and the proposed control scheme is tested for a range of recycling model parameters. As we find the possibility of changing the isotopic mix can be limited for certain unfavorable recycling conditions, we also consider impurity injection as a back-up method for controlling the system. A simple supervisory control strategy is proposed to switch between the primary and back-up control schemes based on stability and performance criteria. A zero-dimensional simulation study is used to study the performance of the control scheme for several scenarios and model parameters. Finally, a one-dimensional simulation is done to test the robustness of the control scheme to spatially varying parameters.

Keywords: nonlinear control, burn control, thermal stability

(Some figures may appear in colour only in the online journal)

1. Introduction

1.1. Motivation

For nuclear fusion to become an economical alternative energy source, tokamak reactors must be capable of operating for extended periods of time in a burning plasma mode characterized by a large value of Q, the ratio of fusion power to auxiliary power. Achieving and maintaining such conditions will require precise control over the plasma density and temperature. Due to the nonlinear and coupled dynamics of the system, regulation of the burn condition (either during ramp-up/shutdown or in response to changing power demands) without a well designed control scheme could result in undesirable transient performance. Feedback control will also be necessary for responding to unexpected changes in plasma confinement, impurity content, or other parameters, which could significantly alter the burn condition during operation. Furthermore, although stable operating points exist for most confinement scalings, certain conditions can lead to thermal instabilities.

[2] Currently at Princeton Plasma Physics Laboratory Princeton, Princeton, NJ 08540, USA

Such instabilities can either lead to quenching or a thermal excursion in which the system moves to a higher temperature equilibrium point. In any of these situations, disruptive plasma instabilities could be triggered, stopping operation and potentially causing damage to the confinement vessel. Thus, it will be important to implement an active feedback control system that can ensure good transient performance as well as stability of the desired operating points.

1.2. Prior work

In past work on the problem of burn condition control, the physical and technological feasibility of various potential actuators has been studied. Prior work, including [1–3], considered auxiliary power, fueling rate, and injection of impurities as possible actuators. While these methods can be effective approaches for burn control, each has unique drawbacks that must be considered when developing a comprehensive burn control strategy.

Controllers based solely on varying auxiliary power [4–6] are best suited for operating points at which the auxiliary power is nonzero, i.e. sub-ignition. The ability of these schemes to reject thermal excursions is restricted since the maximum heating reduction is a complete shutoff of the auxiliary power and the ability to reject thermal quenches is limited by the maximum installed auxiliary heating power. For devices operating with very high fusion gain Q, the amount of auxiliary heating will be quite small compared to the total plasma heating, such that modifying the auxiliary power may have a limited effect on the plasma temperature. In hybrid and steady-state scenarios, the control authority may be further restricted by the need to use some auxiliary power sources to drive plasma current. This essentially forces the burn control system to respect a nonzero minimum auxiliary heating power constraint. Operating points characterized by an auxiliary heating power requirement very close to the minimum required for current drive will be difficult to stabilize and control with auxiliary power regulation alone. Similarly, auxiliary power regulation alone will not be appropriate for future devices exploring ignited operation.

Controller designs based on the controlled actuation of the deuterium-tritium fueling rate, including [7–11], can enable ignited operation (or operation near the minimum auxiliary power required for current drive) by increasing or decreasing the fusion power through changing the plasma density. Due to disruptive density limits, the plasma density cannot be increased arbitrarily high. The approach is also limited by the decay rate of the density, which can be quite slow when particle recycling rates are high. Additionally, the plasma density is nonlinearly coupled to many plasma parameters, such that changes in plasma density could lead to undesirable changes in the reactor operating scenario. The nonlinear coupling is important to consider in control design since, for certain conditions, increasing density results in a net increase in heating while for others, heating is decreased. For example, in [12, 13], where a PID (proportional-integral-derivative) control law was used to regulate fusion power using the deuterium-tritium fueling rate, the sign of the controller gains had to be flipped when switching between thermally stable points and thermally unstable ones, increasing the implementation complexity required to ensure safe operation.

Controlled impurity injection can be used to cool the plasma and prevent thermal excursions. Injecting impurities increases radiative power losses, decreasing fusion heating. Both effects lead to a reduction of the net plasma heating, causing a reduction in temperature. For large perturbations in initial temperature, this method can require large amounts of impurities to be injected. After the excursion, additional heating power, with a consequent reduction in the fusion gain Q, is needed to compensate the excess radiation losses until the impurities are completely removed from the reactor.

Most existing burn control efforts make use of only one of the available actuators (single-input control) and study the range of perturbations that can be rejected by the actuator. Prior work combining actuation concepts include [13–18] for zero-dimensional (volume-averaged) models. Studies of kinetic control and thermal stability for 1D (radial profile) models can be found in [19–21]. In [22], a diagonal multi-input, multi-output linear control scheme for burning plasma kinetics was developed by observing actuator influences during numerical simulations of plasma physics codes. The approximation of the nonlinear burning plasma model by a linearized one for controller design is a common denominator in previous model-based controller designs. The model is linearized, a controller is synthesized using linear techniques, and the resulting design is tested on the original nonlinear model. When tested in nonlinear simulations, these controllers succeed in stabilizing the system against a limited set of perturbations and disturbances.

In our previous work [23], a zero-dimensional nonlinear model involving approximate conservation equations for the energy and densities of the different particles was used to synthesize a nonlinear feedback controller for burn condition stabilization. The controller makes use of all of the previously considered actuators simultaneously, varying the auxiliary power to prevent quenching, impurity injection to increase radiation losses and stop thermal excursions, and varying the fueling to regulate the density to the target value associated with the chosen operating point. The use of nonlinear control techniques removes the limits imposed by linearization in other works and the resulting controller can accommodate very large perturbations. The controller works for suppressing both thermal excursions and quenches, can operate at sub-ignition and ignition points (or points near the minimum power required for current drive), and can drive the system from one point to another during operation. Only those works that use non-model based control techniques, like neural networks [24, 25], have also followed these guidelines. A zero-dimensional (volume-averaged) simulation study was performed to show the capabilities of the model-based controller and compare it with previous linear controllers.

Despite the advantages of the nonlinear controller designed in [23], a few drawbacks remain. The control scheme relies on the use of impurity injection to reject increases in temperature. This type of actuation could lead to undesirable accumulation of impurity ions within the plasma core, which could reduce

the efficiency of the reactor long after the thermal excursion is rejected. Ideally, the injection of impurities would be used only when the other available methods fail to prevent a thermal excursion. Also, the model used for design and simulation assumed an optimal 50:50 mix of deuterium and tritium within the plasma at all times and did not consider the effects of particle recycling. Because experiments indicate that deuterium and tritium may have different transport properties [26], fueling efficiencies, and deposition profiles, and because the isotopic mix in the core affects the amount of fusion heating, the deuterium and tritium systems should be modeled and actuated separately. Additionally, since particle recycling will affect the response of the plasma density and isotopic mix to the available actuators, recycling effects should be included in the model used for design and simulation in some way.

1.3. Isotopic fuel tailoring

The isotopic fuel mix is a critical reactor parameter as it has a major influence on the fusion power produced. The α-particle heating power, P_α, from a burning DT plasma is given as

$$P_\alpha = Q_\alpha \gamma (1-\gamma) n_{\mathrm{DT}}^2 \langle \sigma \nu \rangle \tag{1}$$

where Q_α is the energy of the α-particles produced by the reaction (3.52 MeV),

$$n_{\mathrm{DT}} = n_{\mathrm{D}} + n_{\mathrm{T}} \tag{2}$$

is the deuterium-tritium density, $\langle \sigma \nu \rangle$ is the reactivity, and

$$\gamma = n_{\mathrm{T}}/n_{\mathrm{DT}} \tag{3}$$

is the tritium ratio, a measure of the isotopic mix. We note that for a constant density and temperature, the fusion heating depends quadratically on the tritium ratio, with the maximum fusion power at $\gamma = 0.5$. Even with 50:50 DT injection, the possible differences in deuterium and tritium transport, or fueling deposition and efficiency, may lead to non-optimal fuel mix in the core, which would reduce reactor efficiency. Additionally, depending on the operating scenario, it may be desirable or even necessary to operate at a lower tritium fraction or vary the tritium fraction during operation. Indeed, since the magnitude of the derivative of fusion power with respect to the tritium fraction is zero at $\gamma = 0.5$, control schemes that regulate the fusion power by changing the tritium fraction, like the one proposed in this work, could be more compatible with operation at lower fuel mixes.

To control the tritium ratio it is possible to use a method of fueling referred to as isotopic tailoring, in which the relative mix of deuterium and tritium injected by the fueling system is varied in real-time [27]. The pellet injection system for ITER will include two separate injectors—one with pellets made of primarily deuterium and the other with pellets made primarily of tritium. A gas injection system will be used to supply deuterium at the edge of the plasma. Together, these systems will allow fuel mix regulation. Diagnostics for measuring the tritium ratio in both the edge and core plasma should be available and adequate for the purposes of real-time control [28–31]. Therefore, feedback control of the tritium ratio in ITER plasmas through isotopic fuel tailoring should be feasible.

1.4. Results of this work

In this work, we consider the simultaneous use of auxiliary power, fueling, isotopic fuel tailoring, and impurity injection for stabilizing and controlling a burning plasma. The isotopic fueling technique planned for ITER is used to control the tritium ratio within the plasma. In addition, we exploit the effect of the tritium ratio on the fusion heating power to regulate plasma heating and control the temperature. Doing so allows the proposed scheme to, under certain conditions, maintain control of the plasma temperature when the auxiliary power is saturated without resorting to impurity injection. We note that a non-model based PID (proportional-integral-derivative) algorithm for controlling the isotopic mix was presented in [18], however, varying the isotopic mix as a means of controlling the plasma heating was not considered. For scenarios in which varying the auxiliary power and isotopic mix cannot achieve stability and performance requirements, we propose the use of impurity injection as a back-up actuator to augment the isotopic mix based control. The combined control scheme simultaneously regulates the energy, density, and tritium fraction (and consequently the fusion power), and can, through the use of all of the available actuators, maintain stable control of the system despite saturation of even several of the actuators. The controller synthesis is based on the full nonlinear model, allowing the controller to deal with a larger set of perturbations in initial conditions than linear model based controllers. The controller handles both thermal excursions and quenches and depends parametrically on the equilibrium point, allowing it to be used to drive the system from one equilibrium point to another. The coupling of such a scheme with adaptive control techniques and a real-time optimization algorithm was studied in [32]. In this work, a zero-dimensional simulation study compares the performance of the actively controlled system to the open loop system when switching between operating points, showing a significant improvement in performance. Moreover, a series of simulations is performed to study the effect of different particle recycling model parameters on the performance of the control approach. A one-dimensional simulation study is also done which shows that the control design based on a zero-dimensional model is potentially robust to spatially varying parameters.

1.5. Organization

The burning plasma model is given in section 2. The control objective is described in section 3. In section 4, the controller algorithm is presented. Sections 5 and 6 contain the results of zero-dimensional and one-dimensional simulation studies, respectively. Finally, the conclusions and some plans for future work are given in section 7. Appendices are provided covering the particle recycling model derivation, as well as the basics of Lyapunov stability theory, which is used in the controller design.

2. Burning plasma model

In this work, we use a zero-dimensional model for a burning plasma that employs approximate energy and particle balance equations. The model considers the deuterium and tritium ion

densities separately, allowing for the possibility of different confinement characteristics and fueling rates for the individual species. It also includes an approximate global model of particle recycling for the purposes of studying the effect of recycling parameters on controller performance.

2.1. Particle recycling

The particle balance describing the dynamics of the plasma density and isotopic mix is affected (and under certain conditions dominated) by the recycling of particles from plasma facing components of the confinement vessel walls. An important effect of particle recycling is an increase in the effective confinement time of particles. While a controller can quickly increase the density through increased fueling, the density can be decreased no faster than the effective decay rate, which can be dominated by the recycling effect. Recycling not only poses a problem for actively reducing the total plasma density but may also lead to an increase of helium ash in the core, which could dilute the fusion fuel. In addition, since the recycled fuel will have a particular isotopic mix, recycling reduces the dependence of the core isotopic mix on the controlled pellet and gas injection fueling composition, an effect that was observed in [33]. This could limit the effectiveness of isotopic ratio control schemes.

As one of the goals of this work is to study the feasibility of using manipulation of the isotopic mix and plasma density to control fusion heating in a burning plasma, it is important to include the effects of recycling in the model used for design and simulation. Global models of recycling, like those presented in [34–36], reduce the detailed physical description of the involved processes to a small number of parameters, and can be used to gain a qualitative understanding of the effects of recycling on the system. In this work, we incorporate a parameterized model of coupled deuterium-tritium recycling processes that allows us to study the performance of the proposed controller for a range of different recycling conditions. This model captures the dominant effects of recycling on the proposed isotopic fueling-based control approach, that is, it captures the slowed response time of the deuterium and tritium densities to decreases in fueling and also reflects the fact that the isotopic mix of recycled material may differ from that of the exiting particle flux. Because α particle and impurity ion fluxes are much smaller than the DT flux, recycling of these species is likely to be only weakly coupled to DT recycling and have little effect on the performance of the proposed control approach. We therefore account for α-particle and impurity recycling separately through use of effective confinement times $\tau_\alpha^* > \tau_\alpha$ and $\tau_I^* > \tau_I$. This simplification makes it possible to compare the controller performance for a particular operating point using different DT recycling parameters, without having to simultaneously change the α-particle and impurity recycling conditions, which would alter the fusion power, radiative losses, etc., and significantly change the characteristics of the operating point being studied. Note that the control design approach is not dependent on this modeling choice.

The model of deuterium and tritium recycling used here is based on the following description. Upon leaving the plasma and reaching the vessel walls, a fraction f_{ref} of the exiting particles may be reflected back towards the plasma, while the remainder are either absorbed by the wall material (an effect called wall pumping), or removed from the vessel by the active pumping system. The wall pumping effect causes the development of an inventory of particles in the wall, which is, over time, re-emitted back to the confinement vessel (a small percentage of particles may be trapped more permanently through processes like codeposition [37]). To avoid the need for a complex model of wall conditions and active pumping efficiency, the amount of recycling from the plasma facing surfaces can be characterized by a global recycling coefficient $R^{\text{eff}} = S^{\text{R}}/S^{\text{S}}$, where S^{R} is the recycled particle flux and S^{S} is the particle flux to the plasma facing surfaces. The wall inventory, and consequently the re-emitted particles, will have some isotopic mix, which we denote γ^{PFC}. The recycled (reflected or re-emitted) particles go on to fuel the plasma core with some efficiency, f_{eff}, depending on their energy and interaction with the plasma scrape-off-layer (SOL). The fraction of particles that is 'screened' by the SOL returns to the surface again to be either reflected, absorbed, or pumped out [36]. Based on this description, we can derive (see appendix A) the following expressions for the recycled flux of deuterium and tritium:

$$S_{\text{D}}^{\text{R}} = \frac{1}{1-f_{\text{ref}}(1-f_{\text{eff}})}\left\{f_{\text{ref}}\frac{n_{\text{D}}}{\tau_{\text{D}}} + (1-\gamma^{\text{PFC}})\left[\frac{(1-f_{\text{ref}}(1-f_{\text{eff}}))R^{\text{eff}}}{1-R^{\text{eff}}(1-f_{\text{eff}})} - f_{\text{ref}}\right]\left(\frac{n_{\text{D}}}{\tau_{\text{D}}}+\frac{n_{\text{T}}}{\tau_{\text{T}}}\right)\right\} \tag{4}$$

$$S_{\text{T}}^{\text{R}} = \frac{1}{1-f_{\text{ref}}(1-f_{\text{eff}})}\left\{f_{\text{ref}}\frac{n_{\text{T}}}{\tau_{\text{T}}} + \gamma^{\text{PFC}}\left[\frac{(1-f_{\text{ref}}(1-f_{\text{eff}}))R^{\text{eff}}}{1-R^{\text{eff}}(1-f_{\text{eff}})} - f_{\text{ref}}\right]\left(\frac{n_{\text{D}}}{\tau_{\text{D}}}+\frac{n_{\text{T}}}{\tau_{\text{T}}}\right)\right\} \tag{5}$$

where τ_{D} and τ_{T} are the respective confinement times for the two species.

2.2. Particle and energy balance

The controller design in this work is based on a zero-dimensional particle and energy balance model. The α-particle balance is given by

$$\dot{n}_\alpha = -\frac{n_\alpha}{\tau_\alpha^*} + S_\alpha \tag{6}$$

where n_α is the α-particle density, τ_α^* is the effective confinement time for the α-particles, and

$$S_\alpha = \gamma(1-\gamma)\, n_{\text{DT}}^2 \langle\sigma v\rangle \tag{7}$$

is the source of α-particles from fusion. The deuterium and tritium ion densities are governed by

$$\dot{n}_{\mathrm{D}} = -\frac{n_{\mathrm{D}}}{\tau_{\mathrm{D}}} + f_{\mathrm{eff}} S_{\mathrm{D}}^{\mathrm{R}} - S_{\alpha} + S_{\mathrm{D}}^{\mathrm{inj}} \tag{8}$$

$$\dot{n}_{\mathrm{T}} = -\frac{n_{\mathrm{T}}}{\tau_{\mathrm{T}}} + f_{\mathrm{eff}} S_{\mathrm{T}}^{\mathrm{R}} - S_{\alpha} + S_{\mathrm{T}}^{\mathrm{inj}} \tag{9}$$

where $S_{\mathrm{D}}^{\mathrm{inj}}$ and $S_{\mathrm{T}}^{\mathrm{inj}}$ (controller inputs) are the deuterium and tritium injection rates, respectively. Note that this simplified model of the fueling actuators assumes that the dynamics arising due to transport of the fuel into the core are fast compared to the deuterium/tritium confinement. In [23], these dynamics were approximated by a first order system (justifiable by assuming core transport is dominated by diffusivity [38]), and compensated in a nonlinear control design approach similar to the one used in this work. This compensation approach could easily be added to the control design presented here. Although the controller in this work was designed with the simplified model, preliminary 1D simulations of the control scheme that include the effect of diffusivity are presented in section 6, and show good performance.

We consider two impurity populations: $n_{I,s}$ representing impurities arising from plasma surface interaction and $n_{I,c}$ representing impurities injected for the purposes of burn control. The particle balances are given by

$$\dot{n}_{I,s} = -\frac{n_{I,s}}{\tau_{I,s}^{*}} + S_{I}^{sp} \tag{10}$$

$$\dot{n}_{I,c} = -\frac{n_{I,c}}{\tau_{I,c}^{*}} + S_{I}^{\mathrm{inj}} \tag{11}$$

where $\tau_{I,s}^{*}$ and $\tau_{I,c}^{*}$ are the effective impurity confinement times, S_{I}^{sp} is the uncontrolled source of impurities due to sputtering, and S_{I}^{inj} is the controlled injection of impurities. For the purposes of this work, we model the sputtering source as

$$S_{I}^{sp} = \frac{f_{I}^{sp} n}{\tau_{I,s}^{*}} + f_{I}^{sp} \dot{n} \tag{12}$$

where $0 \leqslant f_{I}^{sp} \ll 1$ in order to maintain $n_{I,s} = f_{I}^{sp} n$ where n is the total plasma density. This simple model reflects the fact that there is typically a small uncontrolled impurity content in the plasma. To simplify presentation, we consider both impurity populations to have the same effective confinement time τ_{I}^{*}, and atomic number Z_{I}. It is straightforward to extend the control design presented here to track each population separately for the general case in which this assumption does not hold. The total impurity content $n_{I} = n_{I,s} + n_{I,c}$ is then governed by

$$\dot{n}_{I} = -\frac{n_{I}}{\tau_{I}^{*}} + S_{I}^{\mathrm{inj}} + S_{I}^{sp} \tag{13}$$

The energy balance is given by

$$\dot{E} = -\frac{E}{\tau_{E}} + P_{\alpha} - P_{\mathrm{rad}} + P_{\mathrm{aux}} + P_{\mathrm{Ohm}} \tag{14}$$

where E is the plasma energy, τ_{E} is the energy confinement time, $P_{\alpha} = Q_{\alpha} S_{\alpha}$ is the alpha-heating ($Q_{\alpha} = 3.52$ MeV is the energy of α-particles), P_{rad} represents the radiation losses, and P_{Ohm} is the ohmic heating power. This model uses the approximation that the 3.52 MeV α-particles slow down instantaneously.

The DT reactivity $\langle \sigma \nu \rangle$ is a highly nonlinear, positive and bounded function of the plasma temperature, T, and is approximated by

$$\langle \sigma \nu \rangle = \exp\left(\frac{a}{T^{r}} + a_{2} + a_{3} T + a_{4} T^{2} + a_{5} T^{3} + a_{6} T^{4} \right) \tag{15}$$

where the parameters a_{i} and r are taken from [39]. In this work, the radiation loss P_{rad} is taken as the combination of bremsstrahlung, line, and recombination as approximated by [40]

$$P_{\mathrm{brem}} = 4.8 \times 10^{-37} \left(n_{\mathrm{D}} + n_{\mathrm{T}} + 4 n_{\alpha} + Z_{I}^{2} n_{I} \right) n_{\mathrm{e}} \sqrt{T(\mathrm{keV})} \tag{16}$$

$$P_{\mathrm{line}} = 1.8 \times 10^{-38} \left(n_{\mathrm{D}} + n_{\mathrm{T}} + 16 n_{\alpha} + Z_{I}^{4} n_{I} \right) n_{\mathrm{e}} (T(\mathrm{keV}))^{-1/2} \tag{17}$$

$$P_{\mathrm{rec}} = 4.1 \times 10^{-40} \left(n_{\mathrm{D}} + n_{\mathrm{T}} + 64 n_{\alpha} + Z_{I}^{6} n_{I} \right) n_{\mathrm{e}} (T(\mathrm{keV}))^{-3/2} \tag{18}$$

where n_{e} is the electron density and Z_{I} is the impurity atomic number. The electron density is obtained from the neutrality condition $n_{\mathrm{e}} = n_{\mathrm{D}} + n_{\mathrm{T}} + 2 n_{\alpha} + Z_{I} n_{I}$. The effective charge, plasma density, and temperature are given by

$$Z_{\mathrm{eff}} = \sum_{i} \frac{n_{i} Z_{i}^{2}}{n_{\mathrm{e}}} = \frac{n_{\mathrm{D}} + n_{\mathrm{T}} + 4 n_{\alpha} + n_{I} Z_{I}^{2}}{n_{\mathrm{e}}} \tag{19}$$

$$\begin{aligned} n &= n_{\alpha} + n_{\mathrm{D}} + n_{\mathrm{T}} + n_{I} + n_{\mathrm{e}} \\ &= 2 n_{\mathrm{D}} + 2 n_{\mathrm{T}} + 3 n_{\alpha} + (Z_{I} + 1) n_{I} \end{aligned} \tag{20}$$

$$T = \frac{2}{3} \frac{E}{n} \tag{21}$$

where Z_{i} is the atomic number of the different ion species. We take $T_{\mathrm{e}} = T_{i} = T$ as a simplification. We approximate the Ohmic heating as [40]

$$P_{\mathrm{Ohm}} = 2.8 \times 10^{-9} \frac{Z_{\mathrm{eff}} I^{2}}{a^{4} T^{3/2}} \tag{22}$$

where I is in Amps and T is in keV.

The state-dependent energy confinement time is given by [41]

$$\tau_{E} = 0.0562 H_{\mathrm{H}} I_{p}^{0.93} B_{\mathrm{T}}^{0.15} P^{-0.69} n_{\mathrm{e19}}^{0.41} M^{0.19} R^{1.97} \epsilon^{0.58} \kappa_{95}^{0.78} \tag{23}$$

where H_{H} is an uncertain scalar that reflects the difficulty of extrapolating to reactor-like parameters, I_{p} is the plasma current (MA), B_{T} is the toroidal magnetic field (T), $P = P_{\mathrm{aux}} + P_{\mathrm{Ohm}} + P_{\alpha} - P_{\mathrm{rad}}$ is the total power within the 95% flux surface (MW), n_{e19} is the electron density (10^{19} m^{-3}), M is the effective mass of the plasma (amu), R is the major radius (m), $\epsilon = a/R$ with a the minor radius (m), and κ_{95} is the elongation at the 95% flux surface/separatrix. We utilize the main plasma parameters and dimensions given in [41] and shown in table 1.

Table 1. ITER machine parameters [41].

Symbol	Description	Value
I	Plasma current	15.0 MA
R	Major radius	6.2 m
a	Minor radius	2.0 m
B	Magnetic field	5.3 T
κ_{95}	Elongation at 95% flux surface/separatrix	1.7
δ_{95}	Triangularity at 95% flux surface/separatrix	0.33
V	Plasma volume	837 m^3

Particle confinement times are assumed to scale with the energy confinement time, i.e.,

$$\tau_\alpha^* = k_\alpha^* \tau_E \tag{24}$$

$$\tau_D = k_D \tau_E \tag{25}$$

$$\tau_T = k_T \tau_E \tag{26}$$

$$\tau_I^* = k_I^* \tau_I \tag{27}$$

We note again that the α-particle and impurity particles balances use effective confinement times chosen to account for recycling, while the confinement times for deuterium and tritium do not, as deuterium-tritium recycling is modeled separately to study the effect of deuterium-tritium recycling model parameters on isotopic mix control.

For the purposes of control, we will consider the states of the burning plasma system to be n_α, n_I, E, γ, and n. The dynamic equations for the first three have already been given in (6), (13), and (14), while, by noting (2), (3), and (20), the remaining two equations can be written as

$$\begin{aligned}\dot{\gamma} = &-\frac{\gamma}{\tau_T} + \frac{\gamma(1-\gamma)}{\tau_D} + \frac{\gamma^2}{\tau_T} \\ &+ \frac{2}{n - 3n_\alpha - (Z_I+1)n_I}\{f_{eff} S_T^R - S_\alpha + S_T^{inj} \\ &- \gamma[f_{eff}(S_D^R + S_T^R) - 2S_\alpha + S_D^{inj} + S_T^{inj}]\}\end{aligned} \tag{28}$$

$$\begin{aligned}\dot{n} = &2\left[-\frac{n - 3n_\alpha - (Z_I+1)n_I}{2}\left(\frac{1-\gamma}{\tau_D} + \frac{\gamma}{\tau_T}\right)\right. \\ &\left. + f_{eff}(S_D^R + S_T^R) - 2S_\alpha + S_D^{inj} + S_T^{inj}\right] + 3\left[-\frac{n_\alpha}{\tau_\alpha^*} + S_\alpha\right] \\ &+ (Z_I+1)\left[-\frac{n_I}{\tau_I^*} + S_I^{inj} + S_I^{sp}\right]\end{aligned} \tag{29}$$

3. Controller objectives

The possible steady-state operating points of the system are given by the equilibria of the dynamic equations (6), (13), (14), (28), and (29). If we consider no controlled injection of impurities at steady-state, i.e. $\bar{S}_I^{inj} = 0$, the equilibrium-point values of the fueling source terms $\bar{S}_D$, $\bar{S}_T$, and the external power $\bar{P}_{aux}$, can be determined by solving the nonlinear algebraic equations

$$0 = -\frac{\bar{n}_\alpha}{\bar{\tau}_\alpha^*} + \bar{S}_\alpha \tag{30}$$

$$\begin{aligned}0 = &-\frac{\bar{\gamma}}{\bar{\tau}_T} + \frac{\bar{\gamma}(1-\bar{\gamma})}{\bar{\tau}_D} + \frac{\bar{\gamma}^2}{\bar{\tau}_T} \\ &+ \frac{2}{\bar{n} - 3\bar{n}_\alpha - (Z_I+1)\bar{n}_I}\{f_{eff}\bar{S}_T^R - \bar{S}_\alpha + \bar{S}_T^{inj} \\ &- \bar{\gamma}[f_{eff}(\bar{S}_D^R + \bar{S}_T^R) - 2\bar{S}_\alpha + \bar{S}_D^{inj} + \bar{S}_T^{inj}]\}\end{aligned} \tag{31}$$

$$\begin{aligned}0 = &2\left[-\frac{\bar{n} - 3\bar{n}_\alpha - (Z_I+1)\bar{n}_I}{2}\left(\frac{1-\bar{\gamma}}{\bar{\tau}_D} + \frac{\bar{\gamma}}{\bar{\tau}_T}\right)\right. \\ &\left. + f_{eff}(\bar{S}_D^R + \bar{S}_T^R) - 2\bar{S}_\alpha + \bar{S}_D^{inj} + \bar{S}_T^{inj}\right] + 3\left[-\frac{\bar{n}_\alpha}{\bar{\tau}_\alpha^*} + \bar{S}_\alpha\right] \\ &+ (Z_I+1)\left[-\frac{\bar{n}_I}{\bar{\tau}_I^*} + \bar{S}_I^{sp}\right]\end{aligned} \tag{32}$$

$$0 = -\frac{\bar{E}}{\bar{\tau}_E} + \bar{P}_\alpha - \bar{P}_{rad} + \bar{P}_{aux} + \bar{P}_{Ohm} \tag{33}$$

$$0 = -\frac{\bar{n}_I}{\bar{\tau}_I^*} + \bar{S}_I^{sp} \tag{34}$$

By specifying $\bar{T}$, $\bar{\gamma}$, and $\bar{\beta}$, (the overbar notation represents steady-state values, $\beta = \frac{knT}{B^2/2\mu_0}$, B is the magnetic field strength, μ_0 is the permeability of free space, and k is the Boltzmann constant), limiting the solution space to physically relevant values of the states (e.g. all states should be positive and not orders of magnitude larger than typical reactor values), using the confinement scaling (23), and iteratively solving, a unique solution to this system can be obtained. We assume the magnetic field B is held constant, such that $\beta \propto nT \propto E$. The objective of a burn condition controller can then be stated as regulation of E, n, γ, n_α and n_I to the chosen set of equilibrium-point values. As a result of regulating these values to the chosen targets, the outputs of the system, including the fusion power, will also be regulated to the value associated with that particular equilibrium point. In this work, the choice of the desired equilibrium point is considered to be made offline prior to the discharge, however, a real-time optimization algorithm could be used to determine the equilibrium that best achieves some predetermined goal, e.g. to maximize fusion gain [32].

We will use the notation $\tilde{x}(t) = x(t) - \bar{x}(t)$ to represent the difference between the actual and desired states of the system. We can write the dynamics of these errors as

$$\dot{\tilde{n}}_\alpha = -\frac{\tilde{n}_\alpha}{\tau_\alpha^*} - \frac{\bar{n}_\alpha}{\tau_\alpha^*} + S_\alpha \tag{35}$$

$$\dot{\tilde{n}}_I = -\frac{\tilde{n}_I}{\tau_I^*} - \frac{\bar{n}_I}{\tau_I^*} + S_I^{\text{inj}} + S_I^{sp} \tag{36}$$

$$\dot{\tilde{E}} = -\frac{\tilde{E}}{\tau_E} - \frac{\bar{E}}{\tau_E} + P_\alpha - P_{\text{rad}} + P_{\text{Ohm}} + P_{\text{aux}} \tag{37}$$

$$\dot{\tilde{\gamma}} = -\frac{\tilde{\gamma}}{\tau_{\text{T}}} + \frac{2[u + (1-\gamma)S_{\text{T}}^{\text{inj}} - \gamma S_{\text{D}}^{\text{inj}}]}{n - 3n_\alpha - (Z_I+1)n_I} \tag{38}$$

$$\dot{\tilde{n}} = -\tilde{n}\left(\frac{1-\gamma}{\tau_{\text{D}}} + \frac{\gamma}{\tau_{\text{T}}}\right) + v + 2(S_{\text{T}}^{\text{inj}} + S_{\text{D}}^{\text{inj}}) \tag{39}$$

where

$$u(\bar{\gamma}) = \frac{n - 3n_\alpha - (Z_I+1)n_I}{2}\left[-\frac{\bar{\gamma}}{\tau_{\text{T}}} + \frac{\gamma(1-\gamma)}{\tau_{\text{D}}} + \frac{\gamma^2}{\tau_{\text{T}}} - \dot{\bar{\gamma}}\right] + f_{\text{eff}} S_{\text{T}}^{\text{R}} - S_\alpha - \gamma[f_{\text{eff}}(S_{\text{D}}^{\text{R}} + S_{\text{T}}^{\text{R}}) - 2S_\alpha] \tag{40}$$

$$v = (-\bar{n} + 3n_\alpha + (Z_I+1)n_I)\left(\frac{1-\gamma}{\tau_{\text{D}}} + \frac{\gamma}{\tau_{\text{T}}}\right) + 2[f_{\text{eff}}(S_{\text{D}}^{\text{R}} + S_{\text{T}}^{\text{R}}) - 2S_\alpha] + 3\left[-\frac{n_\alpha}{\tau_\alpha^*} + S_\alpha\right] + (Z_I+1)\left[-\frac{n_I}{\tau_I^*} + S_I^{\text{inj}} + S_I^{sp}\right] \tag{41}$$

The remainder of this section and the following section on control design rely heavily on the concept of Lyapunov stability, a control design tool used to show the nonlinear stability of equilibrium points of a dynamic system by studying the behavior of a positive definite function of the deviation of the state from the equilibrium point. Throughout the remaining analysis, we will define such functions, referred to as Lyapunov functions, and either show that their derivatives in time are negative definite, indicating asymptotic stability, or choose a feedback control law to ensure that this is the case. More details on this analysis technique are provided in appendix B.

If we consider a Lyapunov function $V_I = \frac{\tilde{n}_I^2}{2}$, then

$$\dot{V}_I = \tilde{n}_I\left(-\frac{\tilde{n}_I}{\tau_I^*} - \frac{\bar{n}_I}{\tau_I^*} + S_I^{\text{inj}} + S_I^{sp}\right) \tag{42}$$

If the total plasma density is regulated to $\bar{n}$, then, by (12), $S_I^{sp} = \frac{f_I^{sp}\bar{n}}{\tau_I} = \frac{\bar{n}_I}{\tau_I}$. Without controlled impurity injection, (42) is reduced to

$$\dot{V}_I\Big|_{\tilde{n}=0} = -\frac{\tilde{n}_I^2}{\tau_I} < 0 \tag{43}$$

Next, we consider a Lyapunov function $V_\alpha = \frac{\tilde{n}_\alpha^2}{2}$, then

$$\dot{V}_\alpha = \tilde{n}_\alpha\left(-\frac{n_\alpha}{\tau_\alpha^*} + S_\alpha\right) \tag{44}$$

If n_I, n, γ, and E are driven to their equilibrium values, we can write

$$S_\alpha = \left[\frac{\bar{n} - 3n_\alpha - (Z_I+1)\bar{n}_I}{2}\right]^2 \bar{\gamma}(1-\bar{\gamma})\langle\overline{\sigma v}\rangle \tag{45}$$

For physically meaningful values of n_α, S_α decreases with an increase in n_α and vice versa. Also, for the confinement scaling (23), the term n_α/τ_α^* increases with an increase in n_α and vice versa. This allows us to write $-\frac{n_\alpha}{\tau_\alpha^*} + S_\alpha = -\tilde{n}_\alpha\phi_\alpha$ where ϕ_α is a positive continuous function and

$$\dot{V}_\alpha\Big|_{\tilde{E},\tilde{n}_I,\tilde{n},\tilde{\gamma}=0} = -\tilde{n}_\alpha^2\phi_\alpha < 0 \tag{46}$$

We can therefore be sure that $\tilde{n}_\alpha$ goes to zero as long as the other states go to zero. Noting (43) and (46), we can restate the control objective as regulation of $\tilde{E}$, $\tilde{n}$, and $\tilde{\gamma}$ to zero. We will achieve this objective through control laws for the auxiliary heating P_{aux}, the fueling terms $S_{\text{D}}^{\text{inj}}$ and $S_{\text{T}}^{\text{inj}}$, and the impurity injection term S_I^{inj}.

4. Controller design

We begin the controller design by looking at the energy subsystem. The dynamic equation (37) can be reduced to

$$\frac{\text{d}\tilde{E}}{\text{d}t} = -\frac{\tilde{E}}{\tau_E} - K_E\tilde{E} \tag{47}$$

where $K_E > 0$ is a design constant, by satisfying the condition

$$f(n, E, n_\alpha, n_I, \gamma, P_{\text{aux}}) = -\frac{\bar{E}}{\tau_E} + P_{\text{Ohm}} + P_\alpha - P_{\text{rad}} + P_{\text{aux}} + K_E\tilde{E} = 0 \tag{48}$$

The $\tilde{E}$ subsystem is then asymptotically stable since $\tau_E > 0$. The condition (48) can be satisfied in several different ways. The auxiliary heating term P_{aux} enters the equation directly, the actuators $S_{\text{D}}^{\text{inj}}$ and $S_{\text{T}}^{\text{inj}}$ can be used to change the α-heating term P_α by modulating the isotopic mix, and the impurity injection term S_I^{inj} can be used to increase the impurity content and consequently P_{rad}. Having several methods available for controlling the energy subsystem enables us to design a control scheme that can still achieve stabilization despite saturation of one or even several of the available actuators.

The control approach proposed in this work integrates all three methods, as needed. In the first two steps, auxiliary heating and a target isotopic mix trajectory γ^* are chosen in such a way that (1) $f = 0$, if this condition is possible using these two methods alone, and (2) $\gamma^* = \bar{\gamma}$ if the auxiliary heating request does not saturate. In step 3, the trajectory γ^* and the equilibrium density $\bar{n}$ are then stabilized through choice of $S_{\text{D}}^{\text{inj}}$ and $S_{\text{T}}^{\text{inj}}$ while avoiding the use of impurity injection. If the system cannot meet stability or performance criteria due to fueling actuator saturation, the controller goes on to step 4, in which a trajectory n_I^* is identified for the impurity density that

can satisfy $f = 0$ and stabilizes this trajectory using impurity injection. The remainder of this section presents the detailed design and analysis of these steps. The final design is demonstrated in simulations in sections 5 and 6.

Step 1: We first calculate P_{aux} as

$$P_{\text{aux}}^{\text{unsat}} = \frac{\bar{E}}{\tau_E} - Q_\alpha \bar{\gamma}(1-\bar{\gamma}) n_{\text{DT}}^2 \langle \sigma v \rangle + P_{\text{rad}} - P_{\text{Ohm}} - K_E \tilde{E} \tag{49}$$

$$P_{\text{aux}} = \text{sat}\left(\frac{P_{\text{aux}}^{\text{unsat}} - P_{\text{aux}}^{\text{min}}}{P_{\text{aux}}^{\text{max}} - P_{\text{aux}}^{\text{min}}} \right) (P_{\text{aux}}^{\text{max}} - P_{\text{aux}}^{\text{min}}) + P_{\text{aux}}^{\text{min}} \tag{50}$$

where the limit $P_{\text{aux}}^{\text{max}}$ depends on the installed power on the tokamak and the limit $P_{\text{aux}}^{\text{min}} \geqslant 0$ depends on the operating scenario.

Step 2: We next find a trajectory γ^* satisfying (48), i.e.

$$Q_\alpha \gamma^*(1-\gamma^*) n_{\text{DT}}^2 \langle \sigma v \rangle - P_{\text{rad}} + P_{\text{Ohm}} + P_{\text{aux}} + K_E \tilde{E} = \frac{\bar{E}}{\tau_E} \tag{51}$$

Solving this equation yields

$$\gamma^*(1-\gamma^*) = \frac{\frac{\bar{E}}{\tau_E} + P_{\text{rad}} - P_{\text{Ohm}} - P_{\text{aux}} - K_E \tilde{E}}{Q_\alpha n_{\text{DT}}^2 \langle \sigma v \rangle} = C \tag{52}$$

$$\gamma^* = \frac{1 \pm \sqrt{1-4C}}{2} \tag{53}$$

This equation is implicit, since C depends on τ_E, which, according to the scaling expression (23), depends on γ through the effective mass M. To overcome this, we can use a fixed-point iteration scheme, i.e.

$$\gamma_n^* = \frac{1 \pm \sqrt{1-4C(\gamma_{n-1}^*)}}{2} \tag{54}$$

and stop the iterations once some tolerance is met. Based on numerical simulation results, very few iterations are needed to achieve convergence, in fact, there is typically little change between the first and second iteration. If the value of P_{aux} calculated in step 1 is not saturated, then $\gamma^* = \bar{\gamma}$. This can be shown by substituting (49) into (51). If $0 \leqslant C \leqslant 0.25$, the two resulting solutions for γ^* are real and we take the tritium-lean solution at each iteration, such that $\gamma^* \leqslant 0.5$. As fusion accounts for most of the heating in a burning plasma, it is unlikely that C would become negative, though this could potentially occur if a very large value of the design constant K_E is chosen. In such a case, the value of K_E could be reduced until $C \geqslant 0$, which would affect response time but not stability, or the value of γ^* could be set to 0 and radiation losses could be used to achieve the required cooling, as described in step 4. If $C \geqslant 0.25$, even the optimal isotopic mix and maximum value of auxiliary heating will not generate enough heating to satisfy $f = 0$, indicating that the requested operating point may not be achievable for the amount of auxiliary heating power installed on the device (the operating point may still be stable even if $f = 0$ is not satisfied and, though not considered here, it could still be possible to achieve $f = 0$ by changing shaping, toroidal field, or plasma current, which influence energy confinement through (23)). Barring this situation, based on our choice of P_{aux} and γ^*, we obtain

$$f(n, E, n_\alpha, n_I, \gamma^*) = 0 \tag{55}$$

This allows us to write $f = \hat{\gamma}\phi_\gamma$ where $\hat{\gamma} = \gamma - \gamma^*$ and ϕ_γ is a continuous function. Noting (37), (48), we can then write the dynamics of the energy perturbation as

$$\dot{\tilde{E}} = -\frac{\tilde{E}}{\tau_E} - K_E \tilde{E} + \hat{\gamma}\phi_\gamma \tag{56}$$

and the dynamics of $\hat{\gamma}$ can be written as

$$\dot{\hat{\gamma}} = -\frac{\hat{\gamma}}{\tau_{\text{T}}} + \frac{2[u(\gamma^*) + (1-\gamma) S_{\text{T}}^{\text{inj}} - \gamma S_{\text{D}}^{\text{inj}}]}{n - 3n_\alpha - (Z_I + 1) n_I} \tag{57}$$

Step 3: Having selected P_{aux} and γ^* in the previous steps, we must next choose $S_{\text{D}}^{\text{inj}}$ and $S_{\text{T}}^{\text{inj}}$ to ensure that $\tilde{E}$, $\hat{\gamma}$, and $\tilde{n}$, which are governed by (56), (57), and (39), are driven to zero. We consider the Lyapunov function $V_0 = V_n + V_{E,\gamma}$ where $V_n = \frac{1}{2}\tilde{n}^2$ and $V_{E,\gamma} = \frac{1}{2}k_1 \tilde{E}^2 + \frac{1}{2}\hat{\gamma}^2$, and look for conditions on $S_{\text{D}}^{\text{inj}}$ and S_{T}^{in} that ensure their derivatives are negative definite, implying asymptotic stability. It can be shown that

$$\dot{V}_n = -\tilde{n}^2 \left(\frac{1-\gamma}{\tau_{\text{D}}} + \frac{\gamma}{\tau_{\text{T}}} \right) + \tilde{n}[v + 2(S_{\text{D}}^{\text{inj}} + S_{\text{T}}^{\text{inj}})] \tag{58}$$

By satisfying

$$2(S_{\text{T}}^{\text{inj}} + S_{\text{D}}^{\text{inj}}) = -v - K_n \tilde{n} \tag{59}$$

where $K_n > 0$, (58) is reduced to

$$\dot{V}_n = -\tilde{n}^2 \left(\frac{1-\gamma}{\tau_{\text{D}}} + \frac{\gamma}{\tau_{\text{T}}} + K_n \right) < 0 \tag{60}$$

guaranteeing $\tilde{n} \to 0$. We then calculate the derivative of $V_{E,\gamma}$ as

$$\begin{aligned} \dot{V}_{E,\gamma} &= k_1 \tilde{E} \left[-\frac{\tilde{E}}{\tau_E} - K_E \tilde{E} + \hat{\gamma}\phi_\gamma \right] \\ &\quad + \hat{\gamma} \left\{ -\frac{\hat{\gamma}}{\tau_{\text{T}}} + \frac{2[u(\gamma^*) + (1-\gamma) S_{\text{T}}^{\text{inj}} - \gamma S_{\text{D}}^{\text{inj}}]}{n - 3n_\alpha - (Z_I + 1) n_I} \right\} \\ &= -k_1 \frac{\tilde{E}^2}{\tau_E} - k_1 K_E \tilde{E}^2 - \frac{\hat{\gamma}^2}{\tau_{\text{T}}} \\ &\quad + \hat{\gamma} \left\{ k_1 \tilde{E}\phi_\gamma + \frac{2[u(\gamma^*) + (1-\gamma) S_{\text{T}}^{\text{inj}} - \gamma S_{\text{D}}^{\text{inj}}]}{n - 3n_\alpha - (Z_I + 1) n_I} \right\} \end{aligned} \tag{61}$$

By satisfying

$$\begin{aligned} (1-\gamma) S_{\text{T}}^{\text{inj}} - \gamma S_{\text{D}}^{\text{inj}} &= -\frac{n - 3n_\alpha - (Z_I + 1) n_I}{2} (k_1 \tilde{E}\phi_\gamma + K_\gamma \hat{\gamma}) \\ &\quad - u(\gamma^*) \end{aligned} \tag{62}$$

where $K_\gamma > 0$, we can reduce (61) to

$$\dot{V}_{E,\gamma} = -k_1\left(\frac{1}{\tau_E} + K_E\right)\tilde{E}^2 - \left(\frac{1}{\tau_T} + K_\gamma\right)\hat{\gamma}^2 < 0 \tag{63}$$

which is negative definite, implying that $\dot{V}_0 < 0$. This guarantees that $\tilde{E}$, $\tilde{n}$, and $\hat{\gamma}$ will be driven to zero. The conditions (59) and (62) can be satisfied by choosing

$$S_D^{inj} = \frac{n - 3n_\alpha - (Z_I + 1)n_I}{2}(k_1\tilde{E}\phi_\gamma + K_\gamma\hat{\gamma}) + u(\gamma^*) + (1-\gamma)\left(\frac{-v - K_n\tilde{n}}{2}\right) \tag{64}$$

$$S_T^{inj} = \left(\frac{-v - K_n\tilde{n}}{2}\right) - S_D^{inj} \tag{65}$$

These values are subject to the constraints $0 \leqslant S_D^{inj} \leqslant S_D^{max}$ and $0 \leqslant S_T^{inj} \leqslant S_T^{max}$. If one of the fueling actuators saturates, we cannot satisfy both conditions of the control law, so we must choose to either control n or γ. If we choose to hold condition (62), the energy and tritium fraction subsystems will remain stable, however, the density subsystem will no longer be controlled. This could potentially lead to a violation of the density limit. To avoid this, we instead choose to maintain control of the density by satisfying (59). Because of fueling actuator saturation, it may be possible that $\dot{V}_{E,\gamma} > 0$, that is, we may not be able to ensure stability of the burn condition with the previously considered actuators. There are two possible situations to consider, either a thermal quench or an excursion. If the system is experiencing a quench, the controller has already increased auxiliary heating to its maximum, so the only alternative would be to change the magnetic plasma parameters to improve energy confinement (see (23)) or to change the reference operating point to one that is achievable. If the system is experiencing a thermal excursion, however, we can still use impurity injection to stabilize the energy subsystem, despite the heating and fueling actuator saturation. In these cases we enable the use of impurity injection by setting the control logic flag $F_{imp} = 1$ and proceeding to step 4.

Step 4: If $F_{imp} = 1$, we use the expression for radiation losses given in (16) to find an impurity density trajectory n_I^* that satisfies condition (48). Defining the error $\hat{n}_I = n_I - n_I^*$, we can write its dynamics as

$$\dot{\hat{n}}_I = -\frac{\hat{n}_I}{\tau_I^*} - \frac{n_I^*}{\tau_I^*} + S_I^{inj} + S_I^{sp} - \dot{n}_I^* \tag{66}$$

Based on the choice of n_I^*, we obtain

$$f(n, E, n_\alpha, \gamma, n_I^*) = 0 \tag{67}$$

which allows us to write $f = \hat{n}_I\phi_I$ where ϕ_I is a continuous function. We can then rewrite (37) as

$$\dot{\tilde{E}} = -\frac{\tilde{E}}{\tau_E} - K_E\tilde{E} + \hat{n}_I\phi_I \tag{68}$$

We take as a Lyapunov function $V_1 = V_n + V_\gamma + V_{E,I}$ where $V_\gamma = \frac{1}{2}\hat{\gamma}^2$ and $V_{E,I} = \frac{1}{2}k_3\tilde{E}^2 + \frac{1}{2}\hat{n}_I^2$.

$$\begin{aligned}\dot{V}_{E,I} &= k_3\tilde{E}\left[-\frac{\tilde{E}}{\tau_E} - K_E\tilde{E} + \hat{n}\phi_n\right] \\ &\quad + \hat{n}_I\left\{-\frac{\hat{n}_I}{\tau_I^*} - \frac{n_I^*}{\tau_I^*} + S_I^{inj} + S_I^{sp} - \dot{n}_I^*\right\} \\ &= -k_3\frac{\tilde{E}^2}{\tau_E} - k_3K_E\tilde{E}^2 - \frac{\hat{n}_I^2}{\tau_I^*} \\ &\quad + \hat{n}_I\left\{k_3\tilde{E}\phi_I - \frac{n_I^*}{\tau_I^*} + S_I^{inj} + S_I^{sp} - \dot{n}_I^*\right\}\end{aligned} \tag{69}$$

By satisfying

$$S_I^{inj} = -k_3\tilde{E}\phi_I + \frac{n_I^*}{\tau_I^*} - S_I^{sp} + \dot{n}_I^* - K_I\hat{n}_I \tag{70}$$

where $K_I > 0$, this can be reduced to

$$\dot{V}_{E,I} = -k_3\left(\frac{1}{\tau_E} + K_E\right)\tilde{E}^2 - K_I\hat{n}_I^2 < 0 \tag{71}$$

guaranteeing $\tilde{E}$ and $\hat{n}_I$ go to zero. We modify the tritium fraction trajectory to $\gamma^* = \gamma^*_{(\text{step 2})} - K_S\int_{t_0}^{t} S_I^{inj}\mathrm{d}t$ where $\gamma^*_{(\text{step 2})}$ is the value of γ^* calculated in step 2, $K_S > 0$, and t_0 is the time at which impurity injection was first engaged. This modification ensures that the tritium fraction is, if possible, eventually reduced to such a level that impurity injection is no longer needed, i.e. $S_I^{inj} \to 0$. Once $S_I^{inj} = 0$, we disable impurity injection in subsequent executions of the algorithm by setting $F_{imp} = 0$. Noting (58) and that

$$\dot{V}_\gamma = \hat{\gamma}\left(-\frac{\hat{\gamma}}{\tau_T} + \frac{2[u(\gamma^*) + (1-\gamma)S_T^{inj} - \gamma S_D^{inj}]}{n - 3n_\alpha - (Z_I + 1)n_I}\right) \tag{72}$$

we can ensure that $\dot{V}_n < 0$, $\dot{V}_\gamma < 0$ by satisfying

$$2(S_T^{inj} + S_D^{inj}) = -v - K_n\tilde{n} \tag{73}$$

$$(1-\gamma)S_T^{inj} - \gamma S_D^{inj} = -\frac{n - 3n_\alpha - (Z_I + 1)n_I}{2}K_\gamma\hat{\gamma} - u(\gamma_I^*) \tag{74}$$

As a result, $\dot{V}_1 < 0$, guaranteeing stability of the system. The conditions (73) and (74) can be satisfied by choosing

$$S_D^{inj} = \frac{n - 3n_\alpha - (Z_I + 1)n_I}{2}K_\gamma\hat{\gamma} + u(\gamma^*) + (1-\gamma)\left(\frac{-v - K_n\tilde{n}}{2}\right) \tag{75}$$

$$S_T^{inj} = \left(\frac{-v - K_n\tilde{n}}{2}\right) - S_D^{inj} \tag{76}$$

which are again subject to saturation. If one of the fueling actuators saturates, we again choose to hold (73) to ensure stability of the density.

Through the proposed control algorithm, values for P_{aux}, S_D^{inj}, S_T^{inj}, and S_I^{inj} are found in such a way that, if possible, the energy and density are driven to the desired values. As the

Table 2. Actuator limits.

Symbol	Description	Value
$P_{\text{aux}}^{\max}$	Maximum power	73 MW
$P_{\text{aux}}^{\min}$	Minimum power	$5/7 \times P_{\text{aux}}^{\max}$
$\dot{P}_{\text{aux}}^{\max}$	Maximum power ramp rate	$2.25 \times 10^4\ \text{Wm}^{-3}\ \text{s}^{-1}$
$S_{\text{D}}^{\max}$	Maximum fueling (D)	$3 \times S_{\text{D}}^{r}$
$\dot{S}_{\text{D}}^{\max}$	Maximum fueling (D) ramp rate	$3 \times 10^{18}\ \text{m}^{-3}\ \text{s}^{-2}$
$S_{\text{T}}^{\max}$	Maximum fueling (T)	$3 \times S_{\text{T}}^{r}$
$\dot{S}_{\text{T}}^{\max}$	Maximum fueling (T) ramp rate	$3 \times 10^{18}\ \text{m}^{-3}\ \text{s}^{-2}$

system approaches the desired operating point and any saturated actuators leave saturation, the trajectories γ^* and n_I^* return to $\bar{\gamma}$ and $\bar{n}_I$, respectively. Once $\tilde{E}$, $\tilde{n}$, and $\tilde{\gamma}$ go to zero, we can be sure, from (43) and (46), that the remaining states $\tilde{n}_\alpha$, and $\tilde{n}_I$ also go to zero.

5. Zero-dimensional simulation study

In this section we study the performance of the proposed control scheme through a zero dimensional simulation study. We use the model described in section 2 for the simulations. We consider magnitude and rate limits on the actuators of the form

$$\begin{aligned} x^{\min} &\leqslant x \leqslant x^{\max} \\ |\dot{x}| &\leqslant \dot{x}^{\max} \end{aligned}$$

where x is a particular actuator. For this study, we use the limits given in table 2. The minimum auxiliary power level was chosen to approximate the situation in which a majority of installed heating power is used to drive current and only the remaining power is available for burn control. In addition to the actuator limits, we limit the feedforward terms $\dot{\gamma}^*$ and $\dot{n}_I^*$ to prevent the controller from reacting to strongly to step changes in these references. We also force $\phi_\gamma = 0$ when $|\hat{\gamma}| < \epsilon$ and $\phi_I = 0$ when $|\hat{n}_I| < \epsilon$, where ϵ is small, so there is no possibility of errors in precision causing ϕ_γ or ϕ_I to become unbounded.

The study is divided into two sections. The first shows how the controller can improve the response of the plasma when moving between operating points, even when the desired operating points are unstable. We then study the effect of recycling model parameters on controller performance. Throughout the simulations, the following parameters are used: $Z_I = 4$, $k_\alpha^* = 7$, $k_I^* = 10$, and $k_{\text{D}} = k_{\text{T}} = 3$.

5.1. Switching between operating points

We begin the simulation study by comparing the open loop (no feedback, actuators set directly according to desired steady-state) and closed loop (feedback controlled) performance of the system when switching between operating points. While more complex open loop control strategies could be generated, their design is out of the scope of this work. Switching between operating points allows us to simultaneously test the response of the nonlinear control scheme to initial perturbations in plasma parameters and to show how, by embedding the nonlinear model of the system in the control scheme, the controller can stabilize a range of operating points. The ability to transition between operating points will be important during reactor startup and shutdown but may also be necessary during operation in order to respond to changes in power load demands or device configuration. For example, if a neutral beam injector malfunctions during operation, the reactor could switch to a different operating point that does not require as much beam power. During such transitions, it will be important to maintain stable control and to avoid large peaks in fusion power or other parameters.

5.1.1. Scenario 1. In this study, we started the system at a set of disturbed initial conditions and requested the plasma to move to an operating point with an auxiliary heating requirement near the power saturation limit $P_{\text{aux}}^{\min}$, then to a second operating point with a higher fusion power and auxiliary heating requirement, and finally to a third operating point again characterized by an auxiliary heating requirement near the saturation limit $P_{\text{aux}}^{\min}$. The operating points during the simulation were given by $[\bar{\beta}_{\text{N}}, \bar{n}, \bar{\gamma}] = [1.96, 1.88 \times 10^{20}/\text{m}^3, 0.38]$ at $t = 0$ s, $[2.05, 1.78 \times 10^{20}/\text{m}^3, 0.4]$ at $t = 75$ s, and $[2.02, 1.86 \times 10^{20}/\text{m}^3, 0.5]$ at $t = 135$ s. The simulations used model parameters $f_I^{sp} = 0.01$, $H_{\text{H}} = 1.13$, $R_{\text{eff}} = 0.9$, $\gamma^{\text{PFC}} = 0.5$, $f_{\text{ref}} = 0.7$, and $f_{\text{eff}} = 0.2$. The initial conditions were set as $n_{\text{D}}(0) = 1.1 \times \bar{n}_{\text{D}}$, $n_{\text{T}}(0) = 1.1 \times \bar{n}_{\text{T}}, n_\alpha(0) = 0.6 \times \bar{n}_\alpha, n_I(0) = \bar{n}_I, E(0) = 0.85 \times \bar{E}$.

The β_{N}, T, n, and P_α results for the open loop and closed loop simulations are compared in figures 1(*a*)–(*d*), respectively. The auxiliary heating, tritium fueling, deuterium fueling, and tritium fraction are shown in figures 2(*a*)–(*d*), respectively. Due to the initial condition perturbation, there was a rapid increase in β_{N} initially in both the open and closed loop cases. This led to an overshoot in both β_{N} and P_α in the open loop case. As reactors may not be tolerant to excursions in β_{N} and P_α, it is important to reduce the overshoot in these quantities. In the controlled case, feedback control law clearly reduced the overshoot and returned the system to the desired operating point. Due to the proximity of the operating point to the auxiliary heating lower saturation limit, the controller was forced to reduce the tritium fraction in order to limit the severity of the excursion. This was accomplished by temporarily reducing the tritium fueling to zero. With more favorable recycling parameters, the controller could have reduced the tritium fraction more quickly and further reduced the overshoot in β_{N} and P_α. At $t = 70$ s, the desired operating point was changed. Again, in the open loop case there was a significant overshoot in β_{N} and P_α, as well as a slow density and temperature response. The system response was greatly improved by the presence of feedback control. Note how the isotopic fueling capability was used to improve the response time of the isotopic mix. At $t = 130$ s, the desired operating point was switched to one that required the minimum auxiliary power.

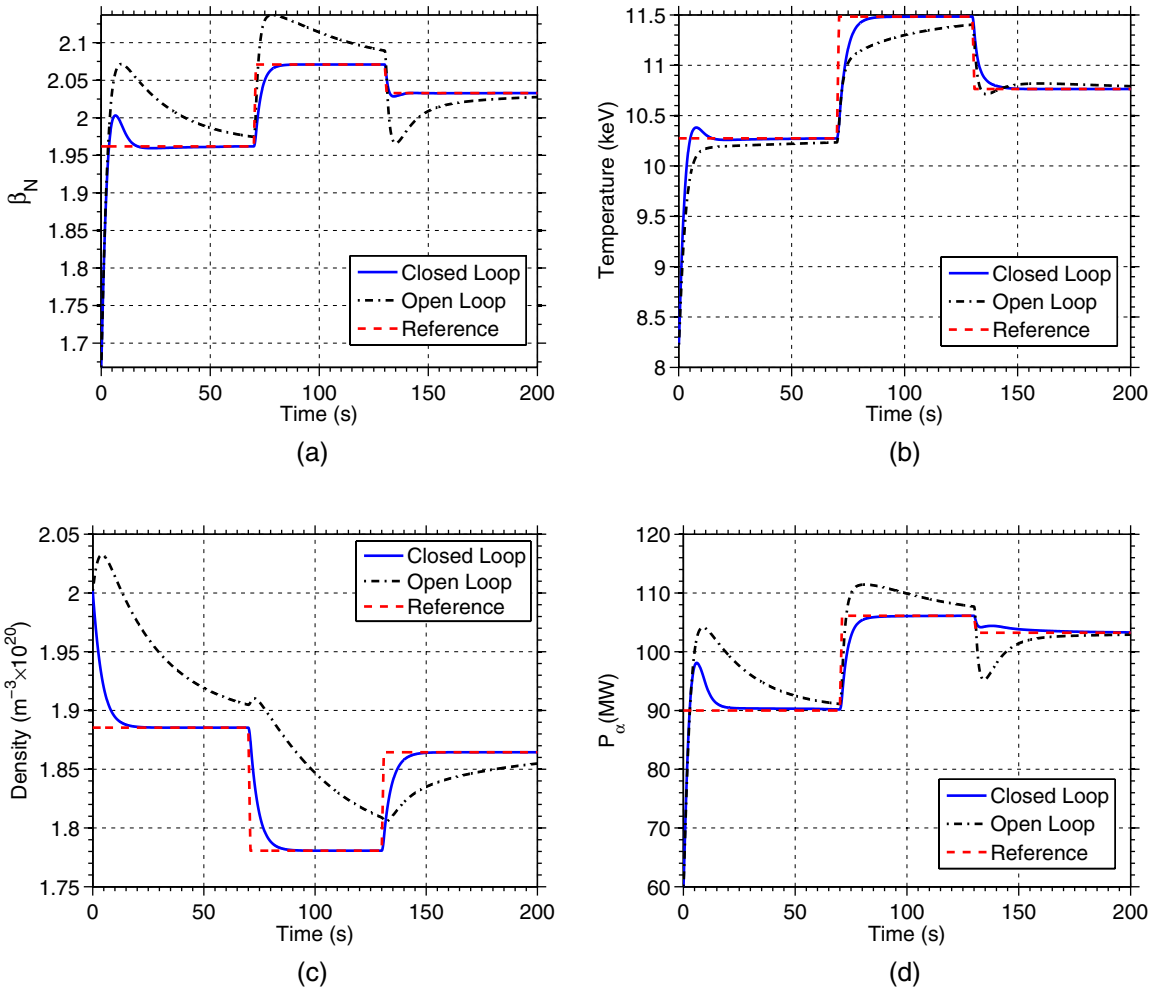

Figure 1. Closed loop, open loop, and desired operating point during the first simulation scenario: (*a*) plasma β, (*b*) plasma density n, (*c*) plasma temperature T, and (*d*) fusion heating P_α.

The open loop case experienced an undershoot in β_N and P_α and a slow density response. The controlled case, on the other hand, quickly tracked the desired β_N, T, and n, and avoided the undershoot in P_α. Because the auxiliary power saturated, the controller altered the tritium fraction to track γ^*. This was done through isotopic fuel tailoring, as seen in figures 2(*b*) and (*c*).

5.1.2. Scenario 2. Next, we considered a second scenario of switching between operating points, this time using an alternative confinement scaling expression. The use of an alternative scaling demonstrates that the design approach can be applied independently of the scaling of confinement with global parameters. It also illustrates the sensitivity of plasma performance to the scaling expression parameters. Specifically, the operating points studied here are unstable in open loop with the alternative scaling expression. We take advantage of this instability to demonstrate the ability of the controller to stabilize unstable operating points, and, in the following sections, to study the controller's effectiveness at rejecting thermal excursions as a function of particle recycling characteristics. In these results, the simulation and controller used the scaling expression ITER90H-P [42]

$$\tau_{E,90H-P} = H_H\, 0.082\, I^{1.02}\, R^{1.6}\, B^{0.15}\, M^{0.5}\, \kappa_{95}^{-0.19}\, P^{-0.47} \qquad (77)$$

We again started the system at a set of disturbed initial conditions and requested the plasma to move to three operating points with auxiliary heating requirements near the power saturation limit $P_{\text{aux}}^{\min}$. The simulations used model parameters $f_I^{sp} = 0.017$, $H_H = 0.75$, $R_{\text{eff}} = 0.9$, $\gamma^{\text{PFC}} = 0.4$, $f_{\text{ref}} = 0.7$, and $f_{\text{eff}} = 0.2$. The operating points during the simulation were given by $[\bar{\beta}_N, \bar{n}, \bar{\gamma}] = [1.8, 2.1\times10^{20}/\text{m}^3, 0.38]$ at $t = 0$ s, $[2.1, 2.1\times10^{20}/\text{m}^3, 0.42]$ at $t = 75$ s, and $[1.8, 2.1\times10^{20}/\text{m}^3, 0.38]$ at $t = 135$ s. The initial conditions were set as $n_D(0) = 1.05\times\bar{n}_D$, $n_T(0) = 1.05\times\bar{n}_T$, $n_\alpha(0) = 0.8\times\bar{n}_\alpha$, $n_I(0) = \bar{n}_I$, $E(0) = 1.1\times\bar{E}$.

The β_N, T, n, and P_α results for the two simulations are compared in figures 3(*a*)–(*d*), respectively. The auxiliary heating, tritium fueling, deuterium fueling, and tritium fraction are shown in figures 4(*a*)–(*d*), respectively. Clearly, with this alternative confinement scaling, the system exhibited much worse open loop performance. The density dropped below the desired level, while β_N and T increased far beyond the requested values. This resulted in a significantly higher fusion heating than desired. These results indicate that the stability

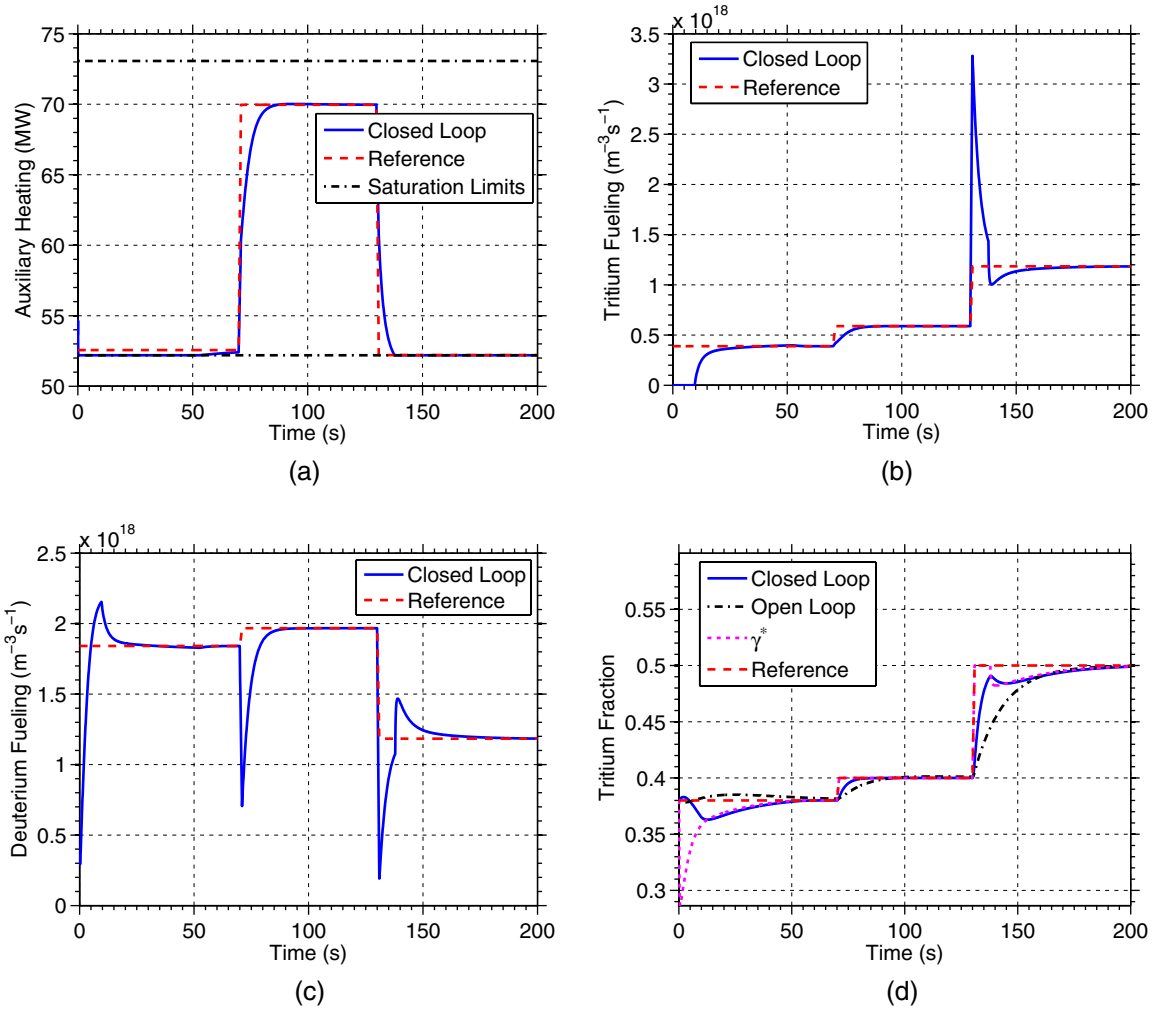

Figure 2. Closed loop and open loop (*a*) heating P_{aux}, (*b*) tritium fueling S_{T}, (*c*) deuterium fueling S_{D}, and (*d*) a comparison of the tritium fraction reference, closed loop and open loop results, and γ^* during the first simulation scenario.

of operating points is strongly affected by the dependence of plasma confinement on changes in other parameters. In the controlled case, the control law accounted for this nonlinear effect, stabilized all three operating points, and achieved excellent transient performance. Because the operating points were so close to the minimum heating power, the controller often saturated the auxiliary heating actuator. The controller reduced γ^* during the heating saturation in order to maintain the reference value of E, and the isotopic fueling capability was used to track this reference. Due to particle recycling the tritium fueling actuator occasionally saturated in an effort to track γ^*, however the overall system performance was still quite good and the criteria for activating impurity injection, i.e. $\dot{V}_{E,\gamma} > 0$ was not violated.

5.1.3. Scenario 3. For a third scenario, we again used the alternative scaling (77). In this case, however, a higher recycling rate was used, making it harder for the controller to track the desired isotopic mix γ^*. The simulations used model parameters $f_I^{sp} = 0.017$, $H_{\text{H}} = 0.75$, $R_{\text{eff}} = 0.95$, $\gamma^{\text{PFC}} = 0.4$, $f_{\text{ref}} = 0.7$, and $f_{\text{eff}} = 0.2$. The same initial conditions as Scenario 2 were used.

The β_{N}, T, n, and P_α results for the open and closed loop simulations of scenario 3 are compared in figures 5(*a*)–(*d*), respectively. The auxiliary heating, tritium fraction, deuterium and tritium fueling, and impurity injection/density are shown in figures 6(*a*)–(*d*), respectively. As in the previous case, the open loop performance was quite poor. In the closed loop simulation, the controller drove the auxiliary heating to saturation several times in order to stabilize the desired operating points. Due to the higher recycling rate, the isotopic mix could not be changed as quickly as in Scenario 2, which prompted the controller to switch to the use of impurity injection (see figures 6(*b*) and (*d*)). The injected impurities cooled the plasma and stabilized the operating points. However, because of the long confinement time of impurities, the impurity density decayed slowly and additional heating power was necessary long after the impurity injection was stopped, as seen in figure 6(*a*).

5.2. Effect of recycling model parameters

The previous simulation scenario showed how, for certain values of the recycling parameters f_{ref}, f_{eff}, and R_{eff}, it can

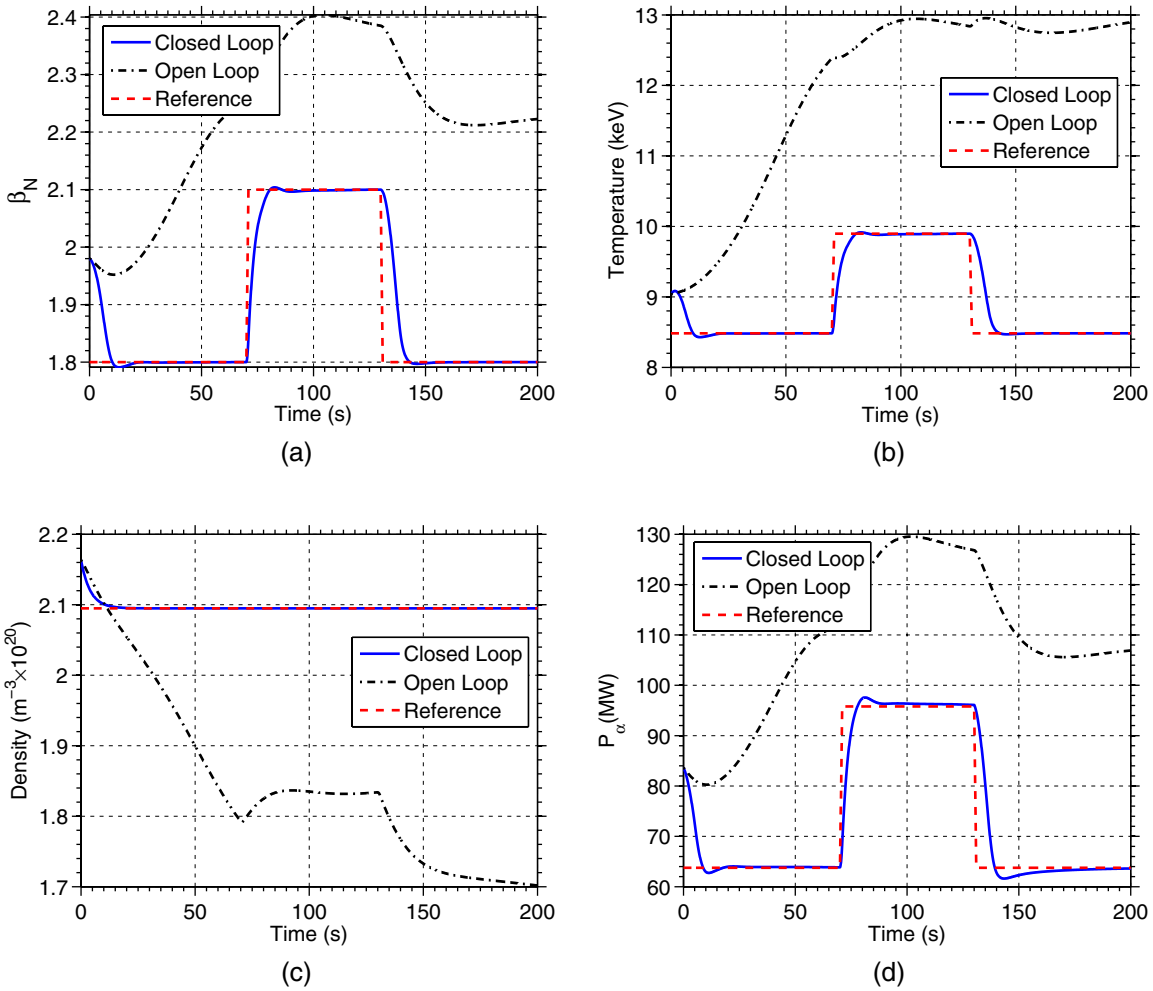

Figure 3. Closed loop, open loop, and desired operating point during the second simulation scenario: (*a*) plasma β, (*b*) plasma density n, (*c*) plasma temperature T, and (*d*) fusion heating P_α.

be difficult to track the stabilizing isotopic mix reference γ^* due to fueling actuator saturation, which degrades the performance of the proposed control scheme and may necessitate the use of impurity injection in some cases. Since the required γ^* depends on the desired operating point and how close it is to the heating actuator saturation limits, any study of the effect of recycling parameters on performance will be highly scenario dependent. Nevertheless, we can get a qualitative understanding of how the parameters influence performance by doing a parametric study for a particular scenario and comparing controller performance metrics. For this study, we chose a scenario ($H_{\rm H} = 1.1$, $\gamma^{\rm PFC} = 0.5$, $f_I^{sp} = 0.015$) in which the controller had to respond to a sudden increase in the confinement parameter $H_{\rm H}$ of 5%, using the scaling (23). The reference for the energy was chosen such that, after the confinement parameter change, the controller was forced to reduce the auxiliary heating to the minimum level and reduce the tritium fraction in order to maintain the desired energy. We used the percent overshoot (the maximum percent difference between the achieved E and the desired value $\bar{E}$), 1% settling time (the time (s) it takes the energy E to come within 1% of its final value), and steady-state error (the difference between the ultimate value of E and the desired value $\bar{E}$) as the controller performance metrics to compare. Again, due to the nonlinearity of the system, the results of this type of study are dependent on the particular scenario studied, but a qualitative sense of how the controller is affected by parameter changes can be gained.

Time evolutions from two illustrative cases are shown in figures 7 and 8. In figure 7, the confinement disturbance at $t = 30$ s causes an excursion in the energy, which the controller responds to by reducing the heating to its lower saturation limit and reducing γ^* to further decrease plasma heating. Over time, adjustment in fueling rates is able to force the tritium fraction to track γ^*, and the energy is forced to its equilibrium value. In figure 8, the recycling model parameters differ in such a way that the the tritium fueling saturates and the controller is unable to track the requested γ^*, resulting in a steady-state error in the energy.

Results of the parametric scan for $R^{\rm eff} = 0.85$, $R^{\rm eff} = 0.90$, and $R^{\rm eff} = 0.95$ are shown in figures 9(*a*)–(*i*), respectively. Each subplot depicts a particular performance metric as a function of $f_{\rm ref}$ and $f_{\rm eff}$. It is apparent that the controller works best for low values of $f_{\rm eff}$ and $R^{\rm eff}$ coupled with high values of $f_{\rm ref}$. For $R^{\rm eff} = 0.85$ there is a large region of parameter space in which there is no steady state error. The region decreases in size as

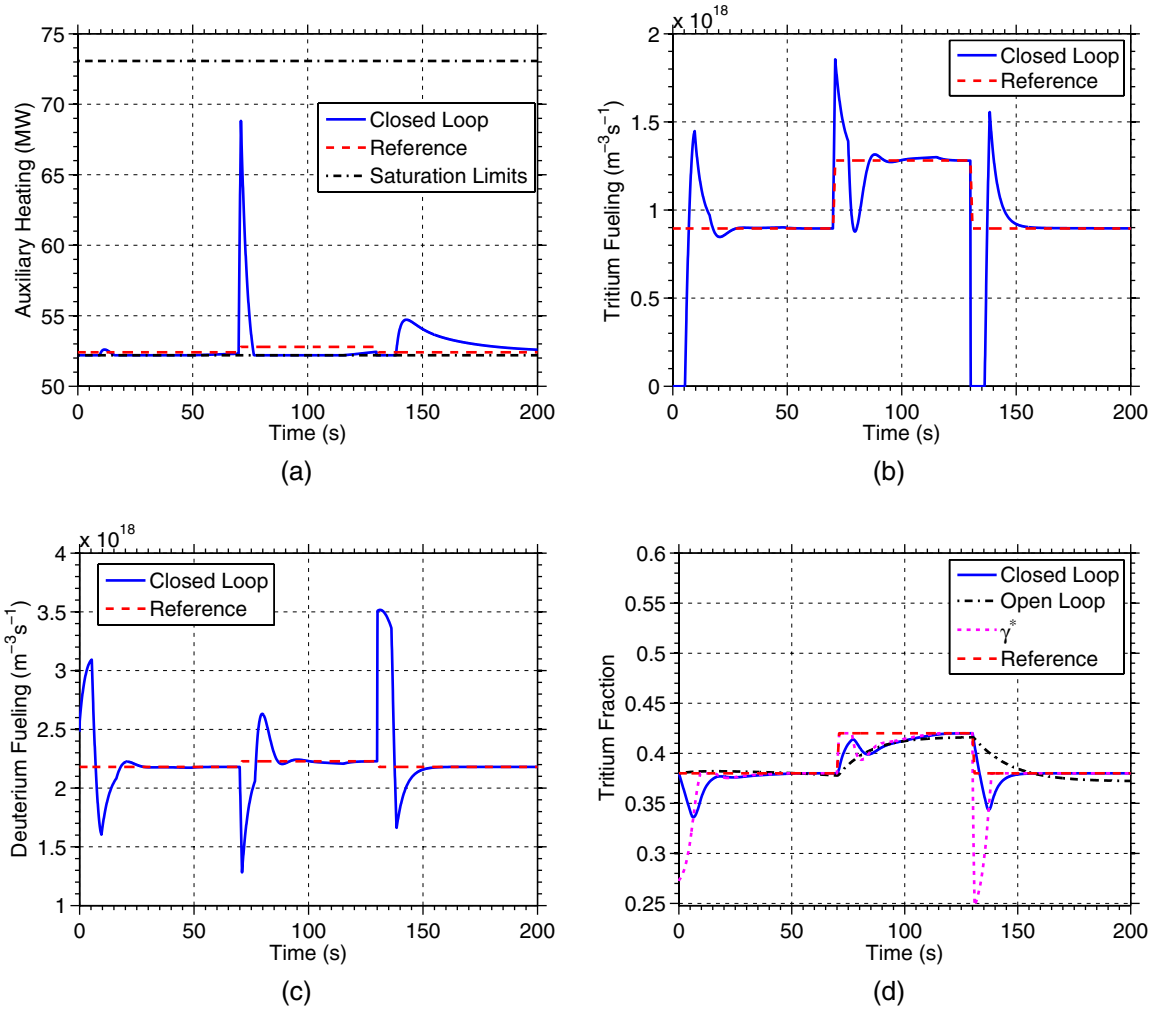

Figure 4. Closed loop (blue, solid) and open loop (red, dashed) (*a*) heating P_{aux}, (*b*) tritium fueling S_{T}, (*c*) deuterium fueling S_{D}, and (*d*) a comparison of the tritium fraction reference, closed loop (blue, solid) and open loop (black, dash-dot) results, and γ^* (magenta, dotted) during the second simulation scenario.

R^{eff} is increased. The overshoot is most strongly dependent on R^{eff} and f_{eff}, though the dependence on f_{ref} increases for high values of f_{eff}. In the region of parameter space without steady-state error, the settling time increases with f_{eff} and decreases with f_{ref}, however, a more complex behavior occurs within the region with steady-state error. The slowest settling time occurs at high values of f_{eff} at the values of f_{ref} where steady-state error begins. In the region with steady-state error, the settling time decreases with decreasing f_{ref}. This complex dependence occurs because, although the response time of the system is slower in this region, the final value of E is closer to the maximum overshoot, so the system takes less time to come to steady-state.

Based on these results, the controller performance is better for lower values of the recycling rate R_{eff} and recycled particle fueling efficiency f_{eff}. Based on experimental studies of a recycling model similar to the one used in this work [36], divertor configurations may be able to achieve quite low values of f_{eff} (<0.5). Divertor designs that prevent recycled flux from escaping the divertor region could be used to reduce f_{eff} while significant active pumping capabilities may be necessary to reduce R_{eff}. The reflectivity f_{ref} is dependent on material properties and the angle at which particles strike the surface. By operating with high reflectivity, the problem of steady-state error can be minimized because the isotopic mix of the recycled material is made less dependent on the content of the walls. As the wall inventory exchanges with the plasma, the isotopic mix of the wall inventory γ^{PFC} may change slowly over time. This would cause the steady-state error seen in these simulations to eventually tend to zero, however, the settling time could be very long since the wall may act as a very large reservoir of particles.

6. One-dimensional simulation study

In this section, we introduce a simplified one-dimensional burning plasma model of the evolution of the radial profiles of the plasma parameters. We use the one-dimensional model to study the performance of the proposed control scheme in the presence of spatially varying parameters. The model is given by the following set of coupled nonlinear partial differential equations:

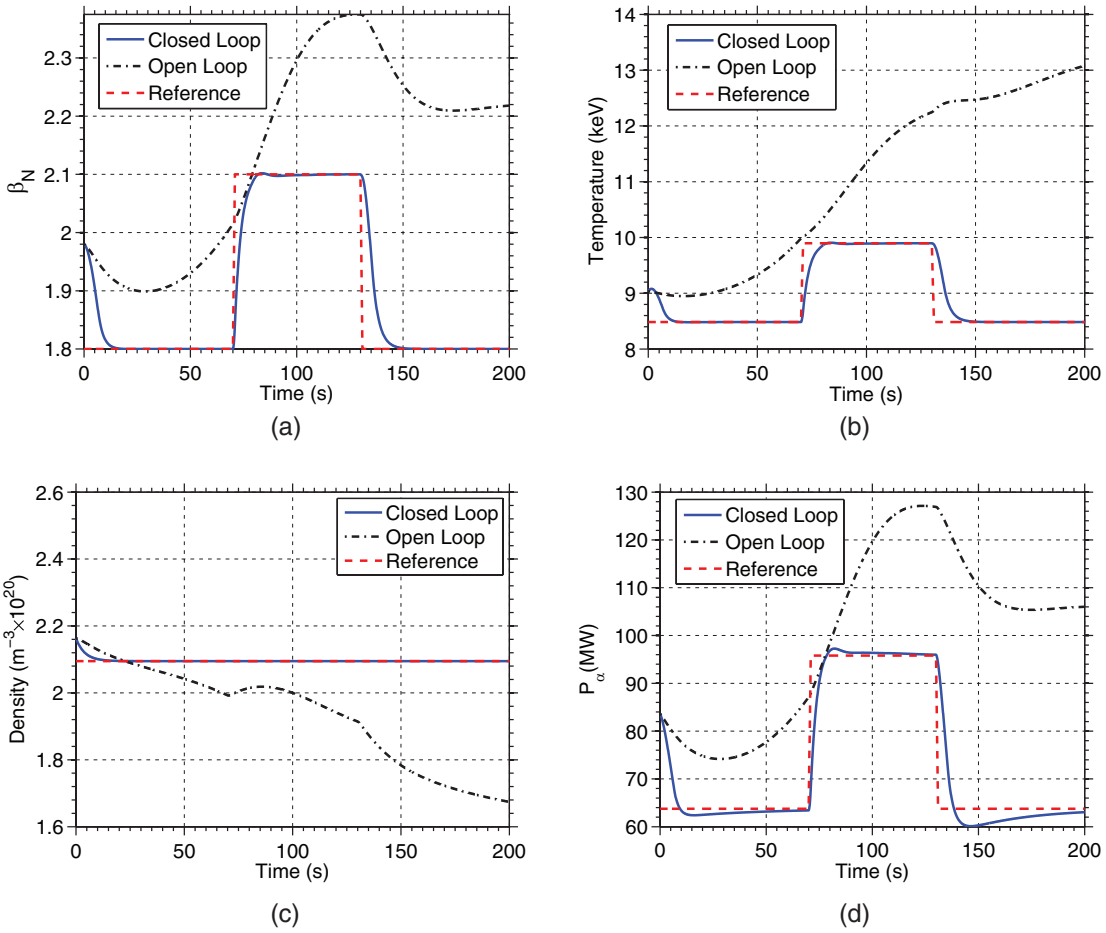

Figure 5. Closed loop, open loop, and desired operating point during the third simulation scenario: (*a*) Plasma β, (*b*) plasma density n, (*c*) plasma temperature T, and (*d*) fusion heating P_α.

$$\frac{\partial n_\alpha(r,t)}{\partial t} = \frac{1}{r}\frac{\partial}{\partial r} r\left(D_\alpha \frac{\partial n_\alpha(r,t)}{\partial r}\right) + S_\alpha(r,t)$$

$$\frac{\partial n_{\mathrm{D}}(r,t)}{\partial t} = \frac{1}{r}\frac{\partial}{\partial r} r\left(D_{\mathrm{D}} \frac{\partial n_{\mathrm{D}}(r,t)}{\partial r}\right) - S_\alpha(r,t) + S_{\mathrm{D}}(r,t) + f_{\mathrm{eff}} S_{\mathrm{D}}^{\mathrm{R}}(r,t)$$

$$\frac{\partial n_{\mathrm{T}}(r,t)}{\partial t} = \frac{1}{r}\frac{\partial}{\partial r} r\left(D_{\mathrm{T}} \frac{\partial n_{\mathrm{T}}(r,t)}{\partial r}\right) - S_\alpha(r,t) + S_{\mathrm{T}}(r,t) + f_{\mathrm{eff}} S_{\mathrm{T}}^{\mathrm{R}}(r,t)$$

$$\frac{\partial n_I(r,t)}{\partial t} = \frac{1}{r}\frac{\partial}{\partial r} r\left(D_I \frac{\partial n_I(r,t)}{\partial r}\right) + S_I(r,t)$$

$$\frac{\partial E(r,t)}{\partial t} = \frac{1}{r}\frac{\partial}{\partial r} r\left(D_E \frac{\partial E(r,t)}{\partial r}\right) + Q_\alpha S_\alpha(r,t) - P_{\mathrm{rad}}(r,t) + P_{\mathrm{Ohm}}(r,t) + P_{\mathrm{aux}}(r,t)$$

where $n_\alpha(r,t)$, $n_{\mathrm{D}}(r,t)$, $n_{\mathrm{T}}(r,t)$, $n_I(r,t)$, and $E(r,t)$ now represent spatially varying model states and $S_\alpha(r,t)$ and $P_{\mathrm{rad}}(r,t)$ are calculated based on local plasma parameter values. This simple cylindrical model assumes constant diffusivities $D_E = 0.3$, $D_{\mathrm{D}} = 0.17$, $D_{\mathrm{T}} = 0.14$, $D_\alpha = 0.10$, $D_I = 0.06$, and negligible pinch velocities. These values are chosen to conceptually study one-dimensional effects and are not based on known physics or empirical values. The heating and fueling rates are distributed throughout the plasma based on the deposition profiles of the respective actuators. We assume the shape of the deposition profiles are fixed in time and only the magnitude of the actuators can be varied by the controller, i.e.,

$$\begin{aligned} S_{\mathrm{D}}(r,t) &= \langle S_{\mathrm{D}}\rangle(t) \times \hat{S}_{\mathrm{D}}(r) \\ S_{\mathrm{T}}(r,t) &= \langle S_{\mathrm{T}}\rangle(t) \times \hat{S}_{\mathrm{T}}(r) \\ S_I(r,t) &= \langle S_I\rangle(t) \times \hat{S}_I(r) \\ P_{\mathrm{aux}}(r,t) &= \langle P_{\mathrm{aux}}\rangle(t) \times \hat{P}_{\mathrm{aux}}(r) \end{aligned}$$

where $\hat{S}_{\mathrm{D}}(r)$, $\hat{S}_{\mathrm{T}}(r)$, $\hat{S}_I(r)$, and $\hat{P}_{\mathrm{aux}}(r)$ are the normalized deposition profiles. The deposition profiles used in this study are shown in figure 10. Profile 1 was used for $\hat{P}_{\mathrm{aux}}(r)$, while Profile 2 was used for $\hat{S}_{\mathrm{D}}(r)$, $\hat{S}_{\mathrm{T}}(r)$, and $\hat{S}_I(r)$. The recycling model used in the zero-dimensional study is used to calculate the recycling rates of deuterium and tritium, and the recycled deuterium and tritium are assumed to fuel the plasma with time-invariant deposition profile, i.e.,

$$\begin{aligned} S_{\mathrm{D}}^{\mathrm{R}}(r,t) &= \langle S_{\mathrm{D}}^{\mathrm{R}}\rangle(t) \times \hat{S}_{\mathrm{D}}^{\mathrm{R}}(r) \\ S_{\mathrm{T}}^{\mathrm{R}}(r,t) &= \langle S_{\mathrm{T}}^{\mathrm{R}}\rangle(t) \times \hat{S}_{\mathrm{T}}^{\mathrm{R}}(r) \end{aligned}$$

where $\langle S_{\mathrm{D}}^{\mathrm{R}}\rangle$ and $\langle S_{\mathrm{T}}^{\mathrm{R}}\rangle$ are calculated using expressions (4) and (5), respectively, and $\hat{S}_{\mathrm{D}}^{\mathrm{R}}(r)$ and $\hat{S}_{\mathrm{T}}^{\mathrm{R}}(r)$ are set as Profile 3 in figure 10.

Based on the cylindrical symmetry of the model, boundary conditions at $r = 0$ are taken as

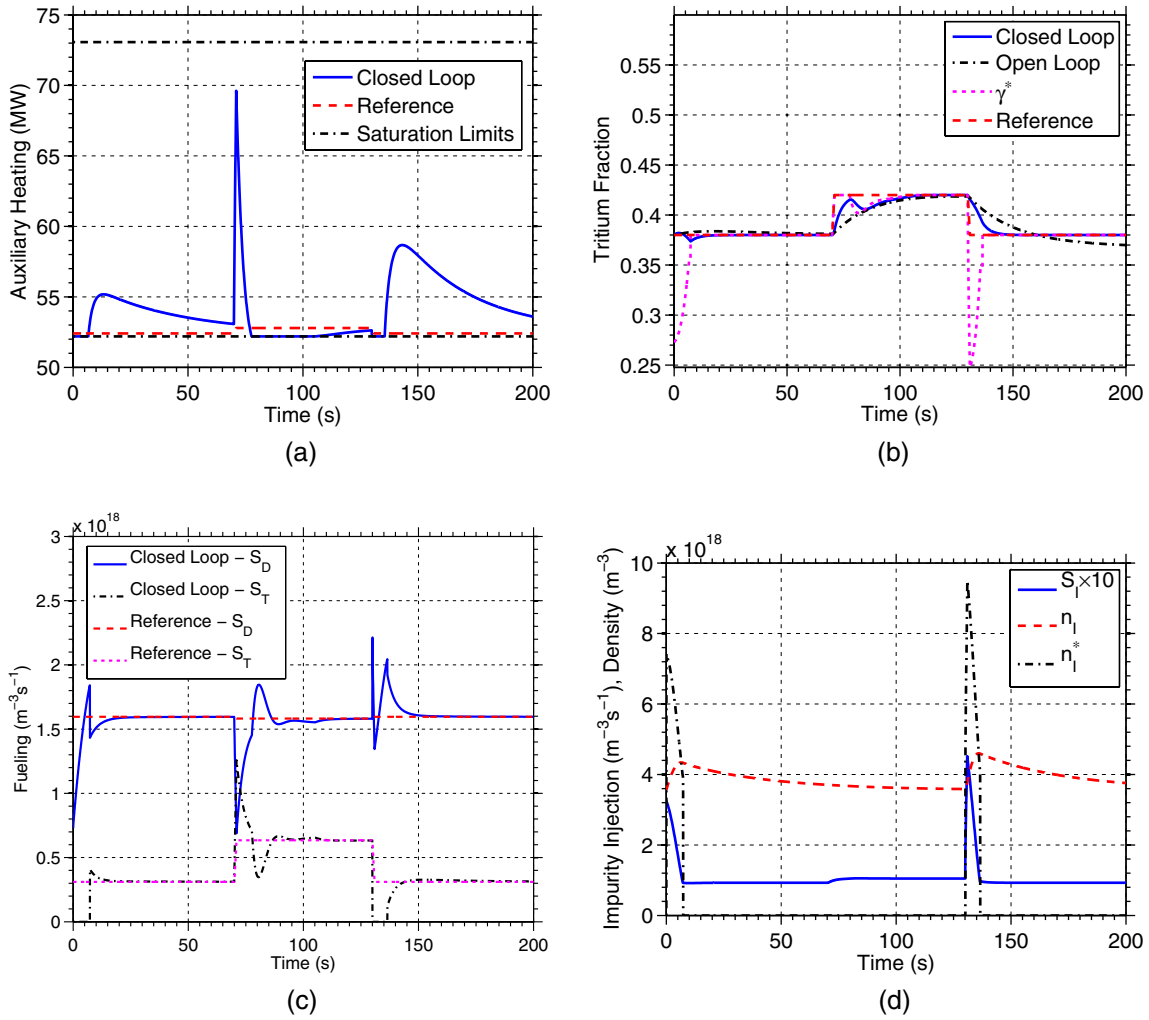

Figure 6. Open and closed loop (*a*) auxiliary heating power, (*b*) tritium fraction, (*c*) deuterium and tritium fueling, and (*d*) impurity injection/density during Scenario 3.

$$\left.\frac{\partial n_\alpha(r,t)}{\partial r}\right|_{r=0}=0,\quad \left.\frac{\partial n_{\rm D}(r,t)}{\partial r}\right|_{r=0}=0,\quad \left.\frac{\partial n_{\rm T}(r,t)}{\partial r}\right|_{r=0}=0,$$
$$\left.\frac{\partial n_I(r,t)}{\partial r}\right|_{r=0}=0,\quad \left.\frac{\partial E(r,t)}{\partial r}\right|_{r=0}=0.$$

For the set of boundary conditions at the minor radius $r = a$, we take

$$\left.\frac{\partial n_\alpha(r,t)}{\partial r}\right|_{r=a}=-d_\alpha n_\alpha(r,t),\quad \left.\frac{\partial n_{\rm D}(r,t)}{\partial r}\right|_{r=a}=-d_{\rm D} n_{\rm D}(r,t),$$
$$\left.\frac{\partial n_{\rm T}(r,t)}{\partial r}\right|_{r=a}=-d_{\rm T} n_{\rm T}(r,t),\quad \left.\frac{\partial n_I(r,t)}{\partial r}\right|_{r=a}=-d_I n_I(r,t),$$
$$\left.\frac{\partial E(r,t)}{\partial r}\right|_{r=a}=-d_E E(r,t),$$

where $d_\alpha = 4.4$, $d_{\rm D} = 1.2$, $d_{\rm T} = 1.6$, $d_I = 1.4$, and $d_E = 4.3$. These values are chosen to conceptually understand one-dimensional effects and are not based on known physics or empirical values.

Volume averaged quantities were obtained from the model through integration. For a quantity $x(r, t)$, its volume average, denoted $\langle x(r,t)\rangle$, is found as

$$\langle x(r,t)\rangle = \frac{2\int_0^a rx(r,t)\mathrm{d}r}{a^2}$$

Furthermore, the confinement time for the quantity $x(r, t)$ can be obtained by computing

$$\tau_x = -\frac{a\langle x(r,t)\rangle}{2D_x\frac{\partial x(r,t)}{\partial r}|_{r=a}} \tag{78}$$

During the closed loop simulation of the 1D model, the diffusivity for each species is updated based on (78) such that the confinement times follow the confinement scaling (23) used in the zero-dimensional study.

During the simulation, the volume averages and confinement times were computed and passed as inputs to the controller, which then output the volume averages of the actuators. We assume that the volume averaged plasma parameters, including $\langle S_\alpha(r,t)\rangle$, $\langle P_{\rm rad}(r,t)\rangle$, and the confinement times are all measured or estimated. To account for the effect of the spatial distribution of parameters, the calculation of γ^* in the step 2 of the control scheme must be modified slightly. We define $\langle\gamma(r,t)\rangle = \langle n_{\rm T}(r,t)\rangle/(\langle n_{\rm T}(r,t)\rangle + \langle n_{\rm D}(r,t)\rangle)$ and write $\langle S_\alpha(r,t)\rangle = f_p^\gamma\langle\gamma(r,t)\rangle(1-\langle\gamma(r,t)\rangle)\langle n_{\rm DT}(r,t)\rangle^2\langle\sigma v\rangle(\langle T(r,t)\rangle)$

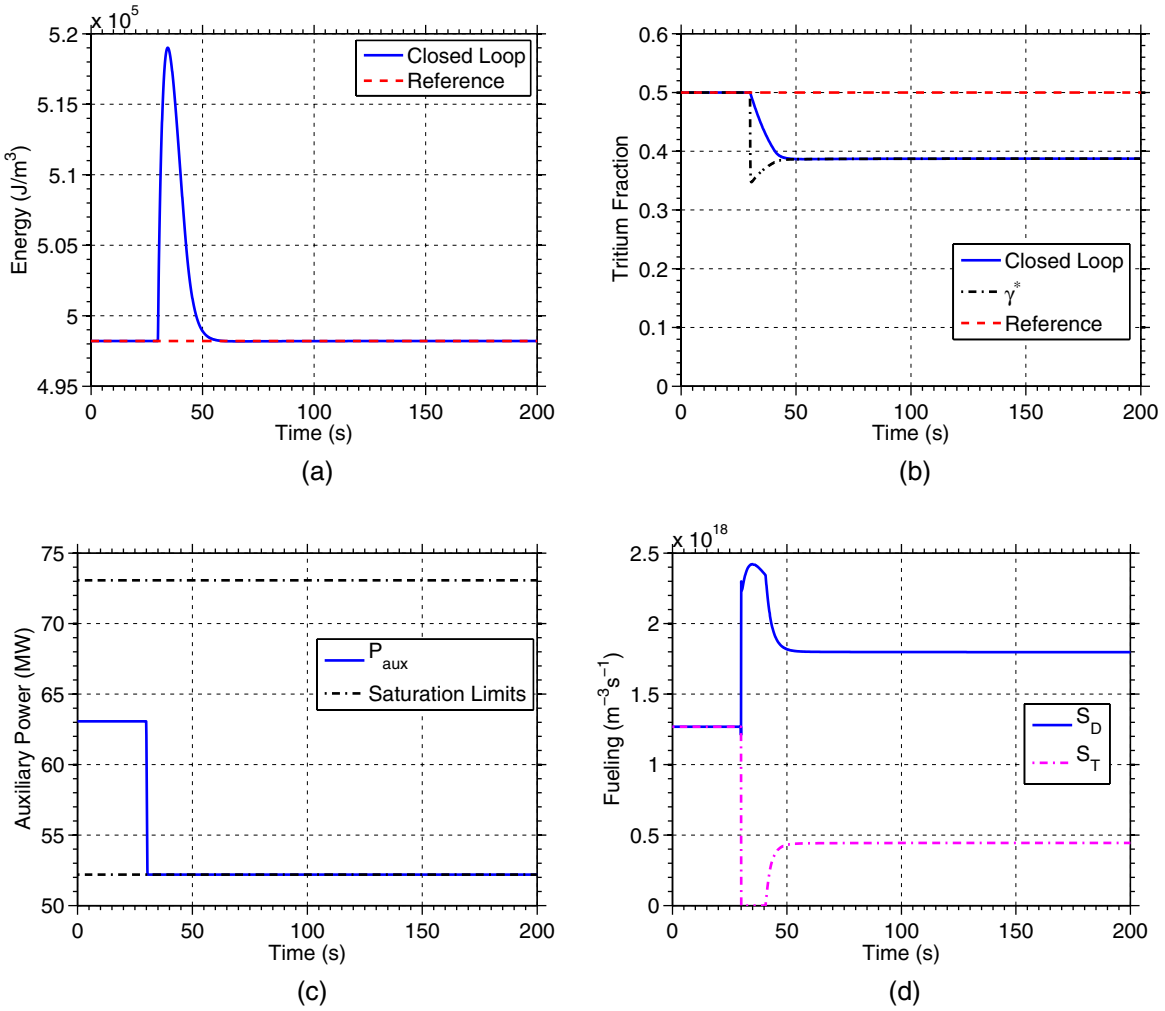

Figure 7. Simulation results for confinement disturbance case with $R_{\text{eff}} = 0.95$, $f_{\text{eff}} = 0.2$, $f_{\text{ref}} = 0.7$. (*a*) Stored energy, (*b*) tritium fraction, (*c*) auxiliary power and (*d*) fueling.

where f_p^{γ} is a scale factor to account for the effects of spatial profiles. The scale factor is then used to calculate

$$\gamma^*(1-\gamma^*) = \frac{\frac{\langle \bar{E}(r,t)\rangle}{\tau_E} + \langle P_{\text{rad}}(r,t)\rangle - \langle P_{\text{Ohm}}(r,t)\rangle + \langle P_{\text{aux}}(r,t)\rangle}{f_p^{\gamma} Q_\alpha \langle n_{\text{DT}}(r,t)\rangle^2 \langle \sigma v\rangle(\langle T(r,t)\rangle)} \equiv \langle C\rangle$$

$$\gamma^* = \frac{1 \pm \sqrt{1-4\langle C\rangle}}{2}$$

The rest of the control scheme is left unchanged, aside from the $\langle\cdot\rangle$ notation, i.e.,

$$\langle P_{\text{aux}}^{\text{unsat}}(r,t)\rangle = \frac{\langle \bar{E}(r,t)\rangle}{\tau_E} - f_p^{\gamma} Q_\alpha \langle \bar{\gamma}(r,t)\rangle(1-\langle \bar{\gamma}(r,t)\rangle) \times \langle n_{\text{DT}}(r,t)\rangle^2 \langle \sigma v\rangle(\langle T(r,t)\rangle) + \langle P_{\text{rad}}(r,t)\rangle - \langle P_{\text{Ohm}}(r,t)\rangle$$

$$\langle S_{\text{D}}^{\text{inj}}(r,t)\rangle = \frac{\langle n(r,t)\rangle - 3\langle n_\alpha(r,t)\rangle - (Z_I+1)\langle n_I(r,t)\rangle}{2} \times (k_{\text{I}}\langle \tilde{E}(r,t)\rangle \phi_\gamma + K_\gamma \langle \hat{\gamma}(r,t)\rangle) + u(\gamma^*) + (1-\langle \gamma(r,t)\rangle)\left(\frac{-\langle v\rangle - K_n\langle \tilde{n}\rangle}{2}\right)$$

$$\langle S_{\text{T}}^{\text{inj}}(r,t)\rangle = \left(\frac{-v - K_n\langle \tilde{n}\rangle}{2}\right) - \langle S_{\text{D}}^{\text{inj}}(r,t)\rangle$$

Actuator limits in the one-dimensional simulation were the same as those used in the zero-dimensional simulation.

For the one-dimensional simulation, a low temperature operating point with an auxiliary heating requirement near the minimum auxiliary power saturation limit was chosen as a reference. Based on the chosen values of $\langle T\rangle$, $\langle \beta\rangle$, and $\langle \gamma\rangle$, as well as the actuator and recycling deposition profiles, the set of equilibrium-point profiles and actuator values associated with the operating point were determined. Two simulations, one using the equilibrium-point fueling and heating rates (open loop) and the other with the proposed controller active (closed loop), were run, both starting from a perturbed set of initial profiles. The parameters used were $H_{\text{H}} = 0.88$, $R_{\text{eff}} = 0.9$, $\gamma^{\text{PFC}} = 0.4$, $f_{\text{eff}} = 1$, and $f_{\text{ref}} = 0.5$. Figure 11 compares the open loop and closed loop volume averages, as well as the spatiotemporal evolution of the percent error, for (*a*) plasma temperature and (*b*) plasma density. Figure 12 shows the same set of results for (*a*) energy and (*b*) fusion heating. The open loop response of the temperature and density to the perturbed initial profiles was quite slow, while in closed loop the desired temperature and density are quickly recovered. In closed loop, the profile percent error tended to zero at all spatial locations with about the same response time as the spatial average values. The energy

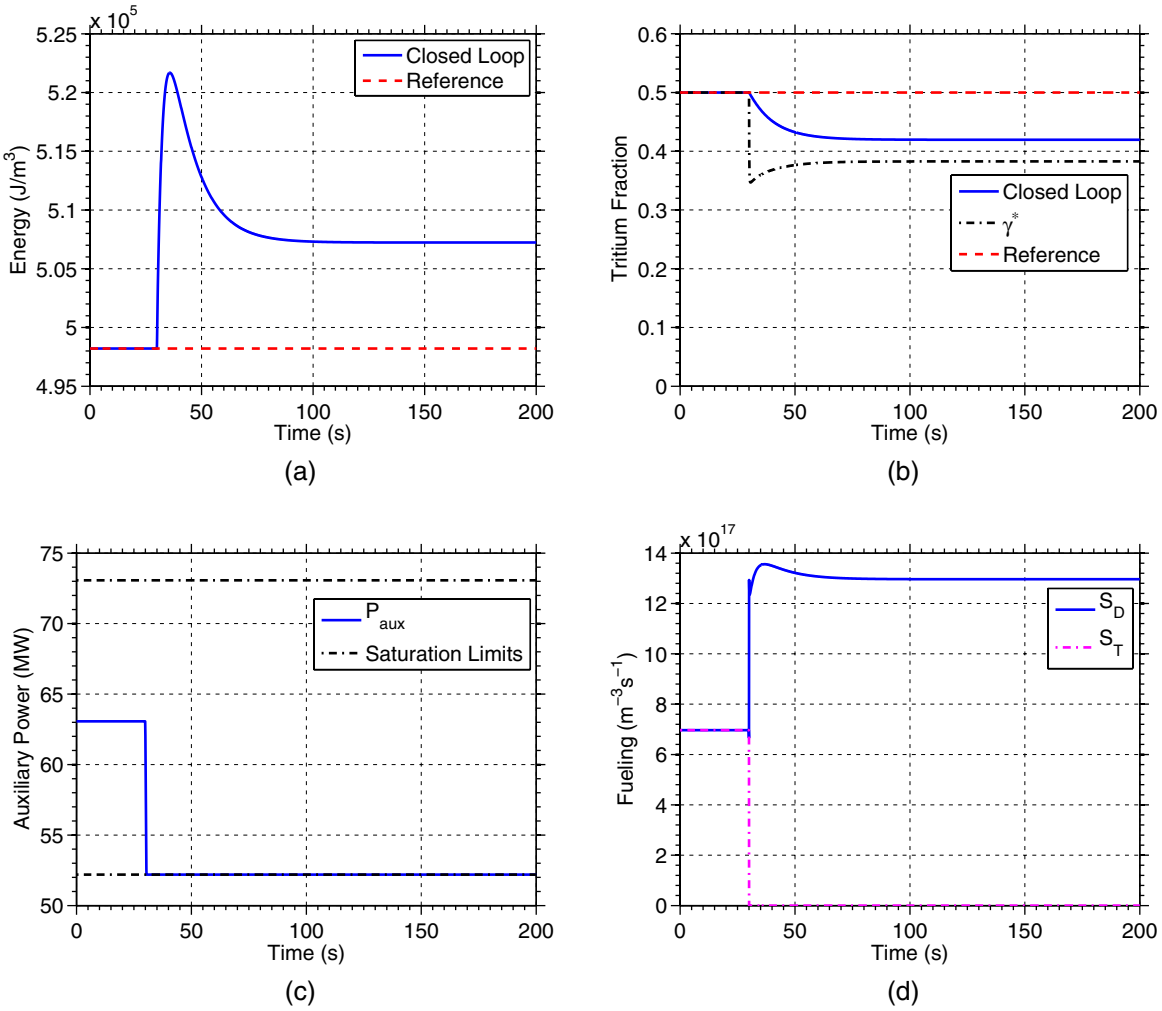

Figure 8. Simulation results for confinement disturbance case with $R_{\text{eff}} = 0.95$, $f_{\text{eff}} = 0.5$, $f_{\text{ref}} = 0.2$. (*a*) Stored energy, (*b*) tritium fraction, (*c*) auxiliary power and (*d*) fueling.

and fusion heating averages initially responded on similar time scales in both open and closed loop. However, the open loop response exhibited an undershoot that persisted for a long time, while the closed loop system quickly reached the desired values. We see similar results in the spatiotemporal evolution of the percent error. Figure 13 compares the open loop and closed loop values of the actuators (*a*) $\langle P_{\text{aux}}(r,t)\rangle$, (*b*) $\langle S_{\text{T}}(r,t)\rangle$, and (*c*), $\langle S_{\text{D}}(r,t)\rangle$, as well as the (*d*) tritium fraction and controller requested tritium fraction γ^*. We see that, because the heating requirement for the operating point was quite close to the minimum saturation limit, the controller could not reduce heating much in response to the initial condition errors. The controller maintained control of the system by requesting a reduction in the tritium fraction γ^*, which was successfully tracked through isotopic fuel tailoring. The open loop tritium fraction did not deviate from the reference value. Finally, figure 14 shows the initial, final ($t = 50$ s), and reference profiles of the states $n_\alpha(r,t)$, $E(r,t)$, $n_{\text{D}}(r,t)$, and $n_{\text{T}}(r,t)$ from the closed loop simulation, showing that, for the simple one-dimensional model used in this work, the profiles tended toward the reference magnitude and shape.

7. Conclusions

We have presented a nonlinear burn stability controller capable of rejecting perturbations in the energy and ion species densities. By avoiding linearization, the controller can deal with a larger set of perturbations than previous linear controllers, and the simultaneous use of multiple actuation techniques allows the rejection of perturbations that lead to either thermal excursions or quenching. The nonlinear control law depends parametrically on the operating point, so it can be used to drive the system between different operating points. This allows online adjustment of the power or other plasma parameters, or transition from sub-ignition to ignition or vice versa. No scheduled controllers or retuning of PID controllers are necessary because the control law is not designed around a particular operating point.

The deuterium and tritium ion densities are accounted for separately, allowing for control of the isotopic fuel mix within the plasma. This will be important for maintaining the desired fuel mix within the plasma core despite difference in confinement properties between the species. The isotopic fueling capability is exploited by the control scheme to help

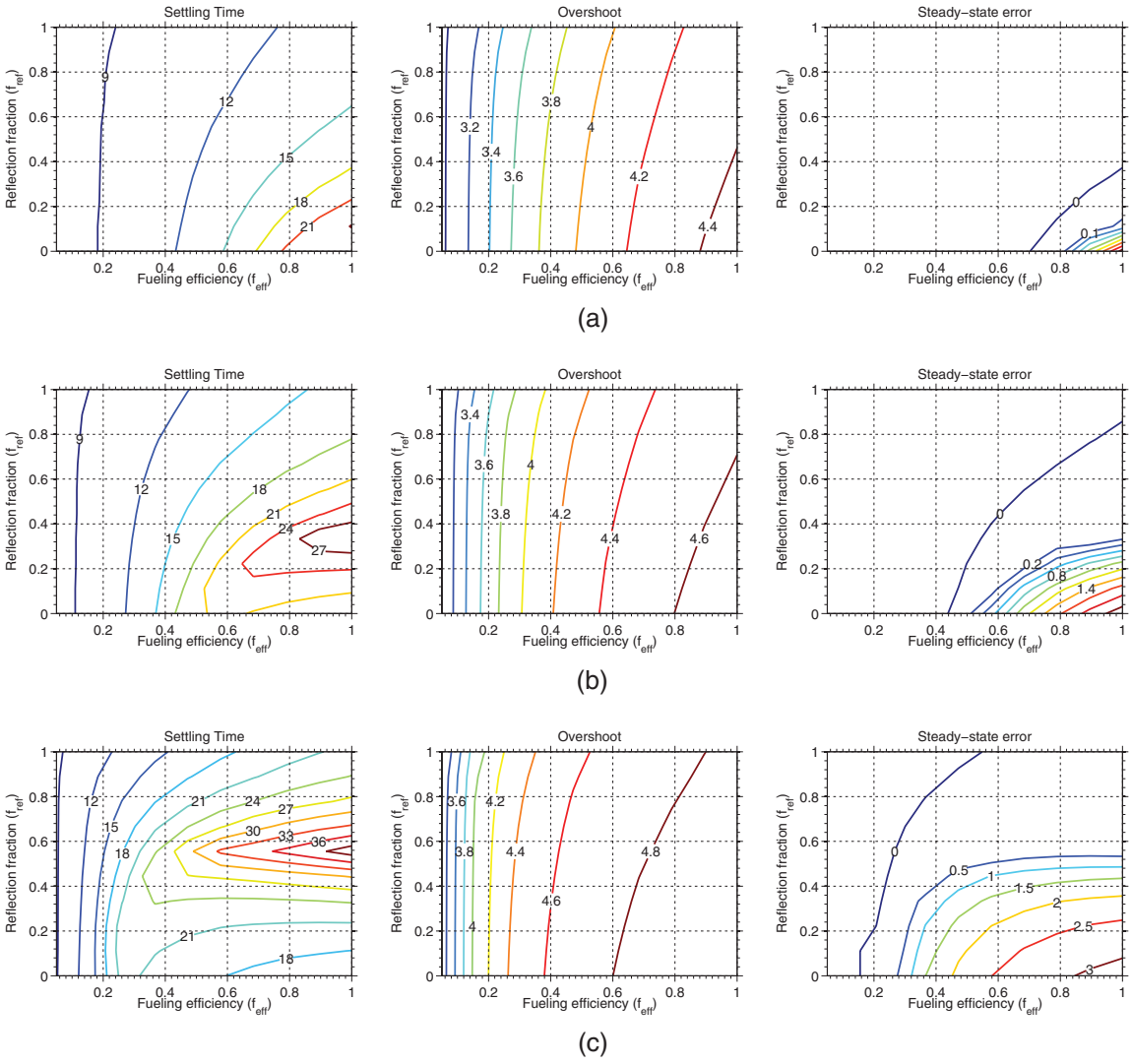

Figure 9. Contour plots of controller performance metrics as a function of recycling parameters for the confinement disturbance scenario with $P_{\text{aux}}^{\text{min}} = (5/7)\bar{P}_{\text{aux}}^{\text{max}}$. All metrics are calculated for the energy state. Settling time is in seconds while overshoot and steady-state error are in %. (*a*) $R^{\text{eff}} = 0.85$, (*b*) $R^{\text{eff}} = 0.90$ and (*c*) $R^{\text{eff}} = 0.95$.

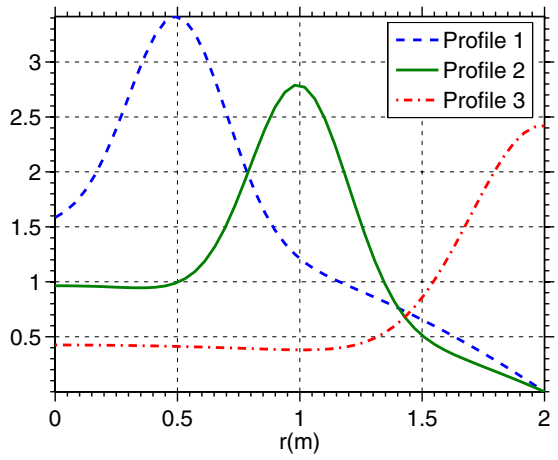

Figure 10. Normalized actuator deposition profiles used in the one-dimensional simulations.

reject perturbations in the temperature when the control law for the heating reaches saturation limits. This extends the operating space of the control scheme and can help to avoid the need for impurity injection during positive temperature perturbations. We include impurity injection in the proposed scheme as a back-up actuator to handle more severe excursions.

A zero-dimensional simulation study was carried out to test the performance of the proposed control scheme. Scenarios studied included moving between various operating points, some of which were characterized by a required heating power very near the minimum power limit imposed in the scenario. Results using two different confinement scalings were shown, demonstrating that the controller is capable of stabilizing unstable operating points, improving the performance of the system for stable operating points, and that the approach is not restricted to a particular confinement scaling. A study of the effectiveness of isotopic mix based control of the energy for a range of recycling model parameters was also presented. The study showed that the use of isotopic fueling for burn condition control purposes is most promising for low values of f_{eff} and relatively low values of R_{eff}. Such favorable conditions could be realized with appropriate divertor design and active

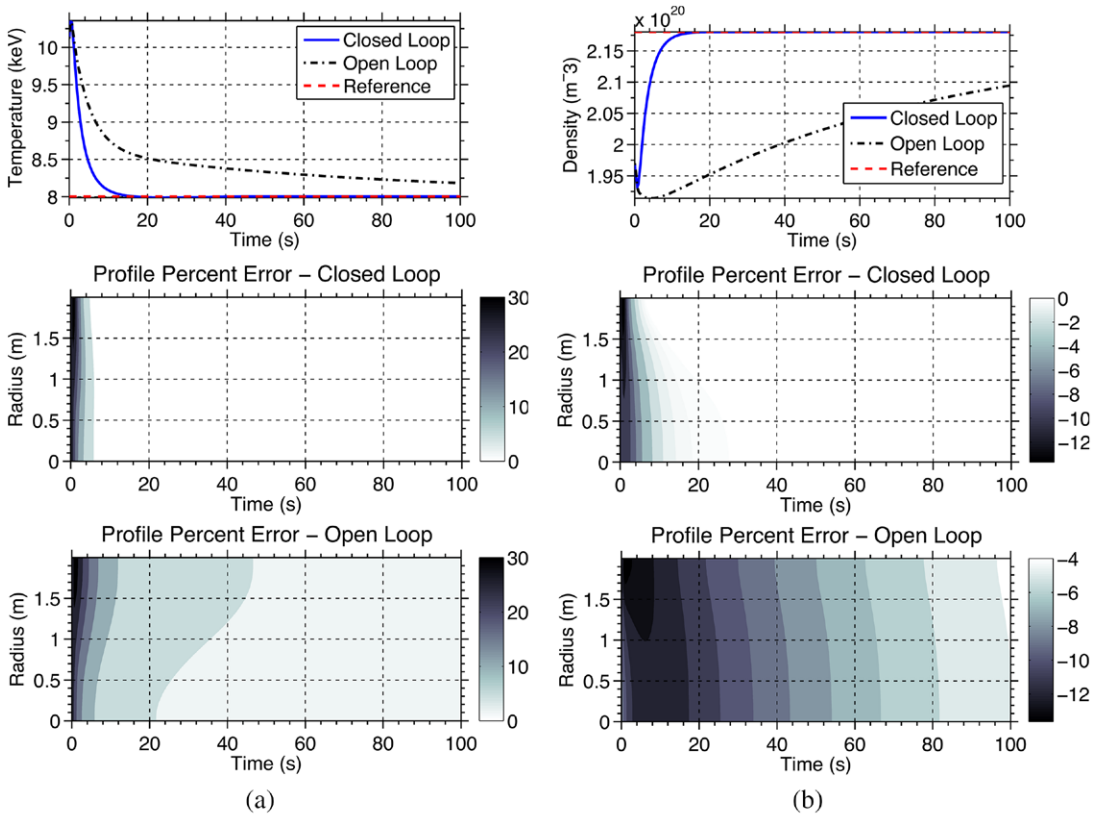

Figure 11. Comparison of closed loop, open loop, and reference volume averages of (*a*) plasma temperature and (*b*) plasma density, along with contour plots depicting the closed loop and open loop spatiotemporal evolution of the percent error of each quantity.

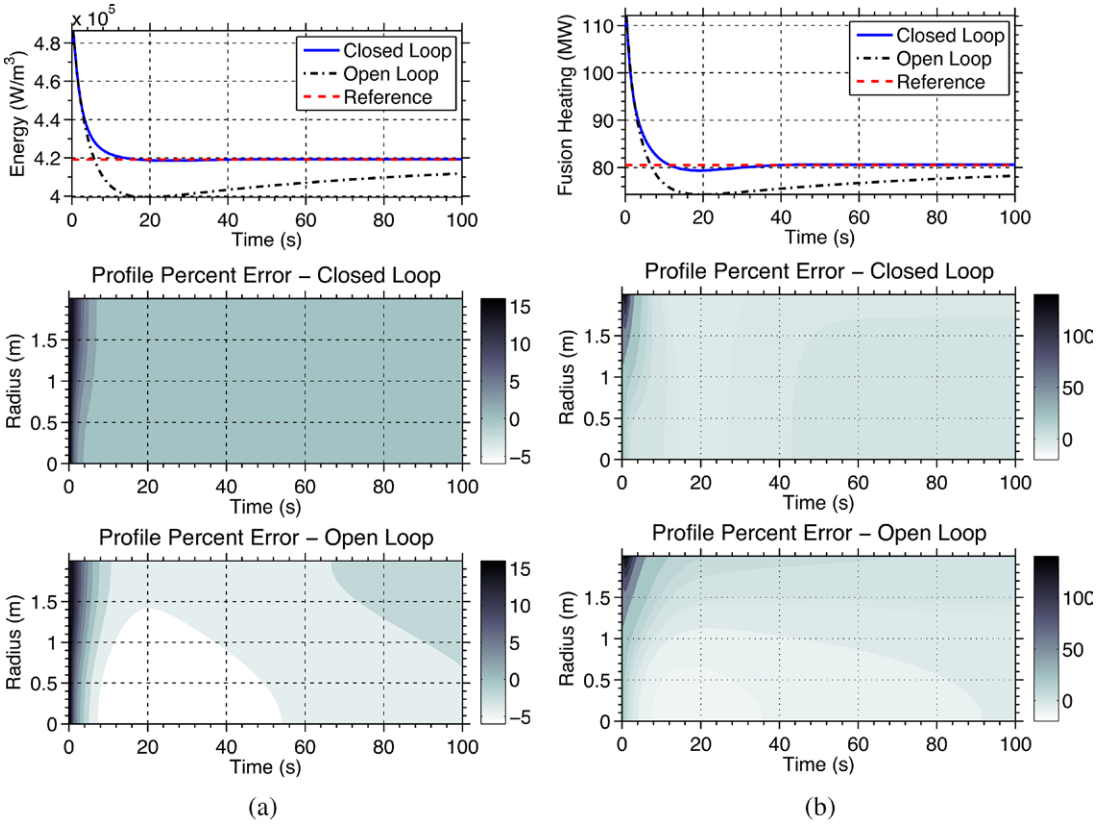

Figure 12. Comparison of closed loop, open loop, and reference volume averages of (*a*) energy and (*b*) fusion heating, along with contour plots depicting the closed loop and open loop spatiotemporal evolution of the percent error of each quantity.

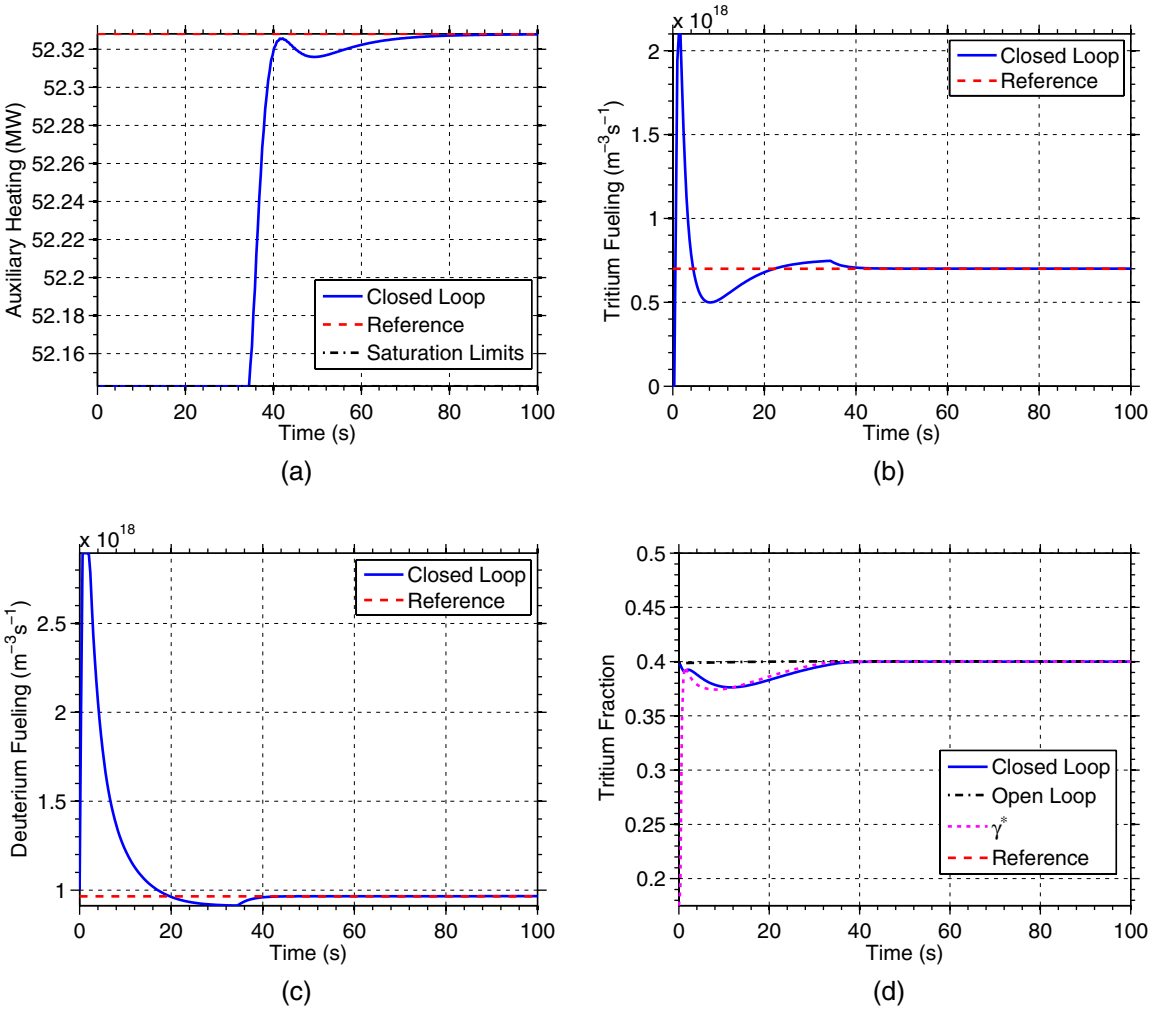

Figure 13. Closed loop and open loop (*a*) heating $\langle P_{\text{aux}}(r,t)\rangle$, (*b*) tritium fueling $\langle S_{\text{T}}(r,t)\rangle$, (*c*) deuterium fueling $\langle S_{\text{D}}(r,t)\rangle$, and (*d*) a comparison of the tritium fraction reference, closed loop and open loop results, and γ^* during the one-dimensional simulation scenario.

pumping capabilities. For unfavorable recycling parameters, it is found that isotopic mix control may be too slow to be used to reject thermal excursions (due to the much faster time scale of the energy subsystem). In such cases, isotopic mix control may still be quite useful for slower time scale regulation of the burn condition and impurity injection may be necessary to reject thermal excursions. A one-dimensional simulation study was also presented to show controller performance when plasma parameters vary in space. Though a very simplified one-dimensional model was used, the success of the zero-dimensional control law on the one-dimensional model is promising and motivates further testing on more complex predictive codes.

We stress that the approach taken in this work is not restricted to the particular confinement scalings and machine parameters used here. The control design could be used in other fusion reactors with isotopic fueling capability. While many of the parameters used in the control law are either measured or well-known, some parameters, like recycling parameters are uncertain. The selection of the controller gains K_E, K_n, K_γ, and K_I, is a trade-off between the robustness of the scheme to these uncertainties and the sensitivity of the controller to noise. In order to handle the the uncertainties in a parametric way, a nonlinear adaptive control law can be synthesized as an augmentation [32] of the proposed controller. A real-time optimization algorithm for updating the choice of operating point parameters $\bar{E}$, $\bar{n}$, and $\bar{\gamma}$ in response to changes in impurity content or confinement parameters can also be included. Such an algorithm, like the preliminary version reported in [32], could be used to optimize the response of parameters like the fusion power and the divertor heat load, while maintaining the stability properties of the controller proposed in this work. Finally, simulation of the proposed scheme using more complex integrated modeling codes, such as TRANSP, CORSICA, or CRONOS, will be used to assess robustness to unmodeled complexities, e.g. actuator dynamics, and the affect of the controller on kinetic profiles and SOL/divertor parameters. Based on these simulations, the control scheme will be tuned, and, if deemed necessary, design changes will be implemented to achieve the desired performance.

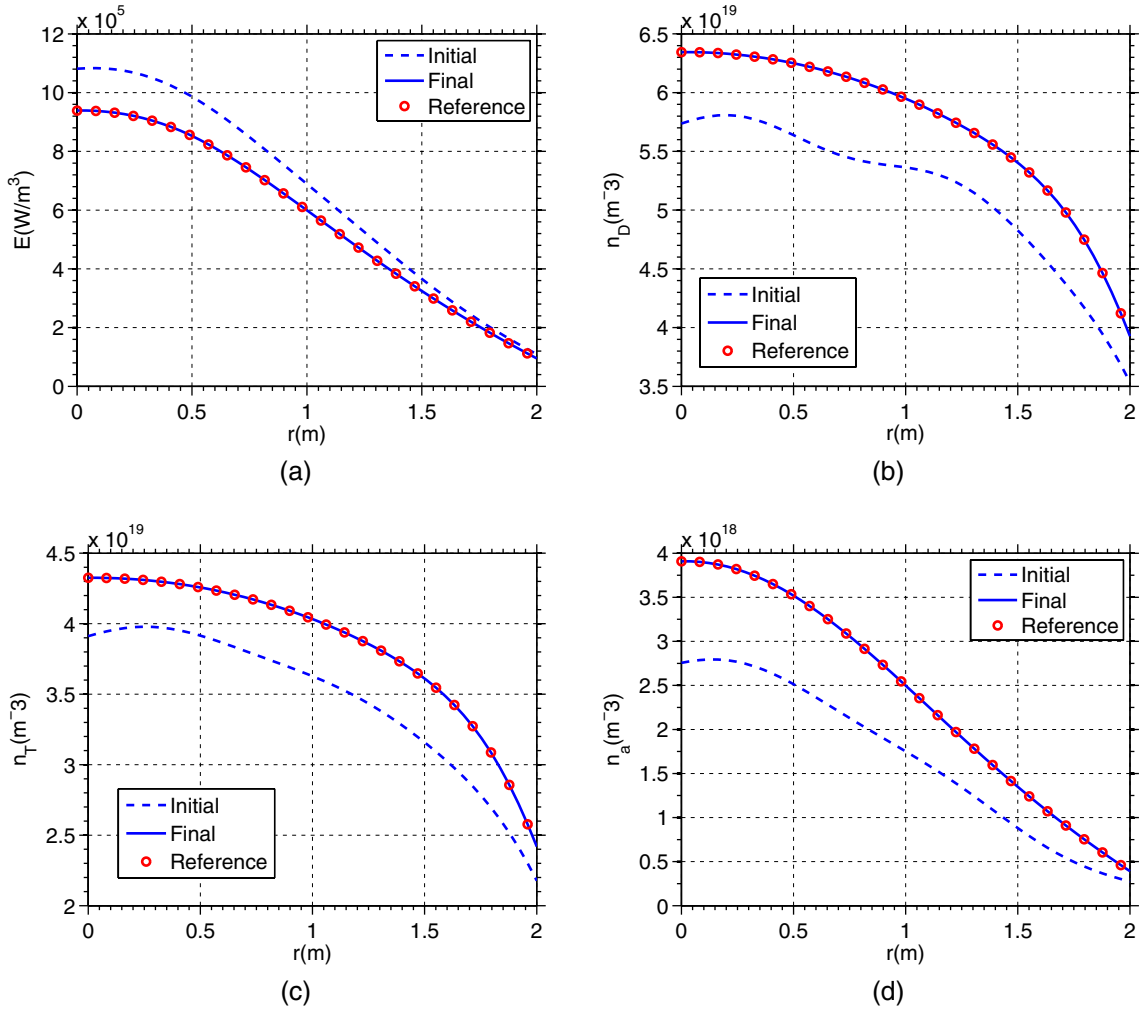

Figure 14. Initial, final ($t = 50$ s), and reference profiles for the one-dimensional closed loop simulation.

Acknowledgments

This work was supported by the National Science Foundation CAREER award program (ECCS-0645086) and by the US Department of Energy under contracts DE-SC0001334 and DE-SC0010661.

Appendix A. Particle recycling model derivation

The following simplified particle recycling model derivation is based on a similar model derived in [36], and extended to include separate equations for deuterium and tritium. The particle balance for deuterium and tritium ions can then be written as

$$\frac{\mathrm{d}n_\mathrm{D}}{\mathrm{d}t} = -\frac{n_\mathrm{D}}{\tau_\mathrm{D}} + f_\mathrm{eff} S_\mathrm{D}^\mathrm{R} + S_\mathrm{D}^\mathrm{inj} \tag{A.1}$$

$$\frac{\mathrm{d}n_\mathrm{T}}{\mathrm{d}t} = -\frac{n_\mathrm{T}}{\tau_\mathrm{T}} + f_\mathrm{eff} S_\mathrm{T}^\mathrm{R} + S_\mathrm{T}^\mathrm{inj} \tag{A.2}$$

where S_D^R and S_T^R represent the total recycling fluxes from the plasma facing components and f_eff is the efficiency with which recycled particles fuel the plasma core. The recycled flux satisfies

$$S_\mathrm{D}^\mathrm{R} = f_\mathrm{ref}\frac{n_\mathrm{D}}{\tau_\mathrm{D}} + (1-\gamma^\mathrm{PFC})S^\mathrm{PFC} + f_\mathrm{ref}(1-f_\mathrm{eff})S_\mathrm{D}^\mathrm{R} \tag{A.3}$$

$$S_\mathrm{T}^\mathrm{R} = f_\mathrm{ref}\frac{n_\mathrm{T}}{\tau_\mathrm{T}} + \gamma^\mathrm{PFC} S^\mathrm{PFC} + f_\mathrm{ref}(1-f_\mathrm{eff})S_\mathrm{T}^\mathrm{R} \tag{A.4}$$

where γ^PFC is the tritium fraction of the particle flux from the plasma facing components, S^PFC, f_ref is the fraction of exiting particles reflected back to the plasma. The first term in each is the reflected flux, the second term is the re-emitted flux, and third term represents the recycled flux that is screened by the plasma due to imperfect core fueling efficiency, and subsequently reflected by the surface. To avoid the need for a self-consistent model of wall implantation, diffusion, and re-emmission to obtain the desorbed flux S^PFC, we simplify the model by considering a recycling coefficient defined as the ratio of total recycling flux to the total flux to the surface, i.e.,

$$R^\mathrm{eff} = \frac{S_\mathrm{D}^\mathrm{R} + S_\mathrm{T}^\mathrm{R}}{S_\mathrm{D}^\mathrm{S} + S_\mathrm{T}^\mathrm{S}} = \frac{S^\mathrm{R}}{S^\mathrm{S}} \tag{A.5}$$

The recycling coefficient includes the effect of wall pumping and active pumping. In order to incorporate the recycling coefficient into the model, we must write an expression for the flux to the surface

$$S_{\mathrm{D}}^{\mathrm{S}} = \frac{n_{\mathrm{D}}}{\tau_{\mathrm{D}}} + (1-f_{\mathrm{eff}})(1-\gamma^{\mathrm{PFC}})S^{\mathrm{PFC}} + f_{\mathrm{ref}}(1-f_{\mathrm{eff}})S_{\mathrm{D}}^{\mathrm{S}} \quad (A.6)$$

$$S_{\mathrm{T}}^{\mathrm{S}} = \frac{n_{\mathrm{T}}}{\tau_{\mathrm{T}}} + (1-f_{\mathrm{eff}})\gamma^{\mathrm{PFC}}S^{\mathrm{PFC}} + f_{\mathrm{ref}}(1-f_{\mathrm{eff}})S_{\mathrm{T}}^{\mathrm{S}} \quad (A.7)$$

where the third term represents the surface flux that is reflected and subsequently returned to the surface due to imperfect fueling efficiency. Since the recycling coefficient compares total hydrogen fluxes, not individual isotopes, we sum (A.3) with (A.4), and (A.6) with (A.7) to obtain

$$S^{\mathrm{R}} = f_{\mathrm{ref}}\left(\frac{n_{\mathrm{D}}}{\tau_{\mathrm{D}}} + \frac{n_{\mathrm{T}}}{\tau_{\mathrm{T}}}\right) + S^{\mathrm{PFC}} + f_{\mathrm{ref}}(1-f_{\mathrm{eff}})S^{\mathrm{R}} \quad (A.8)$$

$$S^{\mathrm{S}} = \frac{n_{\mathrm{D}}}{\tau_{\mathrm{D}}} + \frac{n_{\mathrm{T}}}{\tau_{\mathrm{T}}} + (1-f_{\mathrm{eff}})S^{\mathrm{PFC}} + f_{\mathrm{ref}}(1-f_{\mathrm{eff}})S^{\mathrm{S}} \quad (A.9)$$

We can solve (A.8) and (A.9) to obtain

$$S^{\mathrm{PFC}} = S^{\mathrm{R}}[1-f_{\mathrm{ref}}(1-f_{\mathrm{eff}})] - f_{\mathrm{ref}}\left(\frac{n_{\mathrm{D}}}{\tau_{\mathrm{D}}} + \frac{n_{\mathrm{T}}}{\tau_{\mathrm{T}}}\right) \quad (A.10)$$

$$S^{\mathrm{S}} = \left(\frac{n_{\mathrm{D}}}{\tau_{\mathrm{D}}} + \frac{n_{\mathrm{T}}}{\tau_{\mathrm{T}}}\right) + (1-f_{\mathrm{eff}})S^{\mathrm{R}} \quad (A.11)$$

From the definition of the recycling coefficient, we obtain $S^{\mathrm{S}} = S^{\mathrm{R}}/R^{\mathrm{eff}}$. Substituting this definition into (A.11) and rearranging, we can obtain

$$S^{\mathrm{R}} = \frac{R^{\mathrm{eff}}}{1-R^{\mathrm{eff}}(1-f_{\mathrm{eff}})}\left(\frac{n_{\mathrm{D}}}{\tau_{\mathrm{D}}} + \frac{n_{\mathrm{T}}}{\tau_{\mathrm{T}}}\right) \quad (A.12)$$

Substituting into (A.10) yields

$$S^{\mathrm{PFC}} = \left[\frac{(1-f_{\mathrm{ref}}(1-f_{\mathrm{eff}}))R^{\mathrm{eff}}}{1-R^{\mathrm{eff}}(1-f_{\mathrm{eff}})} - f_{\mathrm{ref}}\right]\left(\frac{n_{\mathrm{D}}}{\tau_{\mathrm{D}}} + \frac{n_{\mathrm{T}}}{\tau_{\mathrm{T}}}\right) \quad (A.13)$$

Solving (A.3) and (A.4) for $S_{\mathrm{D}}^{\mathrm{R}}$ and $S_{\mathrm{T}}^{\mathrm{R}}$, respectively, and substituting (A.13) results in

$$S_{\mathrm{D}}^{\mathrm{R}} = \frac{1}{1-f_{\mathrm{ref}}(1-f_{\mathrm{eff}})}\left\{f_{\mathrm{ref}}\frac{n_{\mathrm{D}}}{\tau_{\mathrm{D}}} + (1-\gamma^{\mathrm{PFC}})\left[\frac{(1-f_{\mathrm{ref}}(1-f_{\mathrm{eff}}))R^{\mathrm{eff}}}{1-R^{\mathrm{eff}}(1-f_{\mathrm{eff}})} - r\right]\left(\frac{n_{\mathrm{D}}}{\tau_{\mathrm{D}}} + \frac{n_{\mathrm{T}}}{\tau_{\mathrm{T}}}\right)\right\} \quad (A.14)$$

$$S_{\mathrm{T}}^{\mathrm{R}} = \frac{1}{1-f_{\mathrm{ref}}(1-f_{\mathrm{eff}})}\left\{f_{\mathrm{ref}}\frac{n_{\mathrm{T}}}{\tau_{\mathrm{T}}} + \gamma^{\mathrm{PFC}}\left[\frac{(1-f_{\mathrm{ref}}(1-f_{\mathrm{eff}}))R^{\mathrm{eff}}}{1-R^{\mathrm{eff}}(1-f_{\mathrm{eff}})} - f_{\mathrm{ref}}\right]\left(\frac{n_{\mathrm{D}}}{\tau_{\mathrm{D}}} + \frac{n_{\mathrm{T}}}{\tau_{\mathrm{T}}}\right)\right\} \quad (A.15)$$

Appendix B. Lyapunov stability basics

In this appendix we review the basics of Lyapunov stability theory, which is crucial to the stability proof in this paper. Consider a nonlinear dynamic system of the form

$$\dot{x} = f(x,u) \quad (B.1)$$

where x (state variable) and u (control input) are vector valued functions of time. We seek a feedback control law of the form

$$u = k(x) \quad (B.2)$$

to achieve a desired property, for example, stability of a certain equilibrium point. A point $x = x_{\mathrm{e}}$ is an equilibrium point of the system when

$$f(x_{\mathrm{e}}, k(x_{\mathrm{e}})) = 0$$

With a shift of the system's origin, i.e, $\tilde{x} = x - x_{\mathrm{e}}$ the equilibrium point can be made to occur at $\tilde{x} = 0$. An equilibrium point $\tilde{x} = 0$ of (B.1) and (B.2) is globally asymptotically stable if there exists a continuously differentiable function $V(\tilde{x})$ such that

$$V(x) > 0 \text{ for all } x \neq 0 \text{ and } V(0) = 0$$

$$V(x) \to \infty \text{ as } |x| \to \infty$$

$$\dot{V} = \frac{\mathrm{d}V}{\mathrm{d}\tilde{x}} f(x, k(x)) < 0 \text{ for all } \tilde{x} \neq 0$$

For example, if we can find a quadratic Lyapunov function $V = \tilde{x}^{\mathrm{T}}P\tilde{x}$ with $\dot{V} = -\tilde{x}^{\mathrm{T}}Q\tilde{x}$, $P, Q > 0$, all of the conditions are satisfied and the equilibrium point x_{e} is asymptotically stable.

The problem of finding a Lyapunov function $V(x)$, even for a system known to be stable, can be very difficult in general. It is often even more difficult when we have to find $V(x)$ and the feedback law $k(x)$ at the same time.

For linear systems, other stability tests exist, for example, Routh–Hurwitz. However, for nonlinear systems such as the one considered in this work, some form of Lyapunov analysis is the only tool available. See [43] for a complete approach to the Lyapunov stability theory.

References

[1] Mandrekas J. and Stacey W.M. 1989 Evaluation of different burn control methods for the International Thermonuclear Experimental Reactor *Proc. 13th IEEE/NPSS Symp. Fusion Engineering (Knoxville, TN)* pp 404–407 (http://ieeexplore.ieee.org/xpls/abs_all.jsp?arnumber=102250)

[2] Haney S., Perkins L.J., Mandrekas J. and Stacey W.M. 1990 *Fusion Sci. Technol.* **18** 606

[3] Anderson D., Elevant T., Hamen H., Lisak M. and Persson H. 1993 *Fusion Sci. Technol.* **23** 5

[4] Bromberg L., Fisher J.L. and Cohn D.R. 1980 *Nucl. Fusion* **20** 203

[5] Chaniotakis E., Freidberg J. and Cohn D. 1989 CIT burn control using auxiliary power modulation *Proc. 13th IEEE/NPSS Symp. Fusion Engineering (Knoxville, TN)* pp 400–403 (doi:10.1109/FUSION.1989.102249)

[6] Haney S. and Perkins L. 1989 Operating point selection and burn stability control for the International Thermonuclear Experimental Reactor *Proc. 13th IEEE/NPSS Symp. Fusion*

Engineering (Knoxville, TN) pp 396–399 (http://ieeexplore.ieee.org/xpl/articleDetails.jsp?arnumber=102248)
[7] Ashby D. and Hughes M.H. 1980 *Nucl. Fusion* **20** 451
[8] Hui W. and Miley G.H. 1992 *Bull. Am. Phys. Soc.* **37** 1399
[9] Hui W., Bamieh B.A. and Miley G.H. 1994 *Fusion Sci. Technol.* **25** 318
[10] Hui W., Fischbach K., Bamieh B.A. and Miley G.H. 1994 Effectiveness, constraints of using the refueling system to control fusion reactor burn *15th IEEE/NPSS Symp. Fusion Engineering (Hyannis, MA)* vol 2 pp 562–4 (doi:10.1109/FUSION.1993.518396)
[11] Plummer D. 1995 Fusion reactor control *Proc. 16th IEEE/NPSS Symp. Fusion Engineering (Champaign, IL)* vol 2 pp 1186–9 (doi:10.1109/FUSION.1995.534438
[12] Mitarai O., Sagara A., Ohyabu N., Sakamoto R., Komori A. and Motjima O. 2009 *Fusion Sci. Technol.* **56** 1495
[13] Mitarai O., Sagara A., Sakamoto R., Ohyabu N., Komori A. and Motojima O. 2010 *Plasma Fusion Res.* **5** S1001
[14] Sestero A. 1983 *Fusion Sci. Technol.* **4** 437–51
[15] Mitarai O. and Muraoka K. 1999 *Nucl. Fusion* **39** 725
[16] Mitarai O. and Muraoka K. 1999 *Fusion Sci. Technol.* **36** 194
[17] Sager G., Miley G. and Maya I. 1985 *Fusion Sci. Technol.* **8** 1795
[18] Mitarai O. 2002 Fuel ratio and fueling control for safe ignited operation in ITER class Tokamak reactors *Advances in Plasma Physics Research* vol 2 (Huntington, NY: Nova Science Publishers) p 37
[19] Firestone M.A. and Kessel C.E. 1991 *Plasma Phys.* **19** 29–41
[20] Miley G. and Varadarajan V. 1992 *Fusion Sci. Technol.* **22** 425
[21] Fuchs V., Shoucri M.M., Thibaudeau G., Harten L. and Bers A. 1983 *IEEE Trans. Plasma Sci.* 411–18
[22] Leonov V.M., Mitrishkin Y.V. and Zhogolev V.E. 2005 Simulation of burning ITER plasma in multi-variable kinetic control system *32nd EPS Conf. on Plasma Physics (Tarragona, Spain)* vol 29 pp 2–5
[23] Schuster E., Krstic M. and Tynan C. 2003 *Fusion Sci. Technol.* **43** 18
[24] Vitela J. 2001 *Plasma Phys. Control. Fusion* **43** 99
[25] Vitela J. 1998 *Plasma Phys. Control. Fusion* **40** 295
[26] Zastrow K.D., Adams J.M., Baranov Y.F., Belo P., Bertalot L. and Others A. 2004 *Plasma Phys. Control. Fusion* **46** B255
[27] Gouge M.J., Houlberg W.A., Attenberger S.E. and Milora S.L. 1995 *Fusion Sci. Technol.* **28** 1644–50
[28] Baylor L., Parks P., Jernigan T., Caughman J., Combs S., Foust C., Houlberg W.A., Maruyama S. and Rasmussen D. 2007 *Nucl. Fusion* **47** 443
[29] Asai K., Naoi N., Iguchi T., Watanabe K., Kawarabayashi J. and Nishitani T. 2006 *J. Nucl. Sci. Technol.* **43** 320
[30] Okada K., Kondo K., Kubota N., Ochiai K., Sato S., Nishitani T., Konno C., Okamoto A., Kitajima S. and Sasao M. 2007 *Plasma Fusion Res.* **2** S1083
[31] Dudok de Wit T., Duval B., Joye B. and Lister J. 2011 *Nucl. Fusion* **31** 359
[32] Boyer M.D. and Schuster E. 2014 *Plasma Phys. Control. Fusion* **56** 104004
[33] Owens D.K. *et al* 1995 *J. Nucl. Mater.* **220–2** 62–72
[34] Hirooka Y., Masuzaki S., Suzuki H., Kenmotsu T. and Kawamura T. 2001 *J. Nucl. Mater.* **290–3** 423–7
[35] Maddison G., Turner A., Fielding S.J. and You S. 2006 *Plasma Phys. Control. Fusion* **48** 71
[36] Ehrenberg J. 1996 *Physical Processes of the Interaction of Fusion Plasmas with Solids* (New York: Academic) p 35
[37] Andrew P. *et al* 1999 *J. Nucl. Mater.* 266–9 153
[38] Santiago E., Witrant E., Goniche M. and Clairet F. 2011 An optimal feedback approach to particle source identification in tokamaks *Proc. of the 15th IEEE Int. Conf. on System Theory, Control and Computing (Sinaia, Romania)* pp 1–7 (http://ieeexplore.ieee.org/xpl/login.jsp?tp=&arnumber=6085744&url=http%3A%2F%2Fieeexplore.ieee.org%2Fxpls%2Fabs_all.jsp%3Farnumber%3D6085744)
[39] Hively L. 1977 *Nucl. Fusion* **17** 873–6
[40] Stacey W.M. 2010 *Fusion: An Introduction to the Physics and Technology of Magnetic Confinement Fusion* 2nd edn (New York: Wiley)
[41] ITER 2001 Summary of the ITER final design report, *Technical Report*, (Vienna: IAEA)
[42] Uckan N. 1994 Confinement capability of ITER-EDA Design *15th IEEE/NPSS Symp. Fusion Engineering (Hyannis, MA)* vol 1 p 183–6 (doi:10.1109/FUSION.1993.518311
[43] Khalil H. and Grizzle J. 1996 *Nonlinear Systems* 2nd edn (Englewood Cliffs, NJ: Prentice Hall)